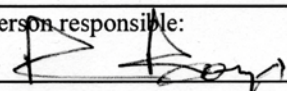


GEOLOGI FOR SAMFUNNET

GEOLOGY FOR SOCIETY



Report no.: 2010.025		ISSN 0800-3416	Grading: Confidential until 20.04.2012	
Title: Microscope and SEM (scanning electron microscope) investigations of thin sections from the Nussir copper deposit				
Authors: Jan Sverre Sandstad		Client: Nussir ASA		
County: Finnmark		Commune: Kvalsund		
Map-sheet name (M=1:250.000) Honningsvåg		Map-sheet no. and -name (M=1:50.000) 1935 I Repparfjorden		
Deposit name and grid-reference: Nussir, 35W 390500 7818100		Number of pages: 55	Price (NOK):	
Fieldwork carried out:		Date of report: 20.04.2010	Project no.: 263100	Person responsible: 
<p>Summary:</p> <p>16 polished thin sections have been prepared from core samples from four drill holes from the eastern part of the Nussir Cu deposit with enrichments of Ag, Au, Pt and Pd. The main aims of the study were to describe the various copper-sulphide minerals and to identify noble metal-bearing minerals and their relationship to the copper sulphides. Some of the polished thin sections have been investigated by use of scanning electron microscope (SEM) and semi-quantitative analyses have been performed.</p> <p>The host rocks of the Nussir deposit are fine-grained sandstones and siltstones that contain carbonate-rich layers. They are heterogeneously deformed, and both rocks with well-preserved primary layering and rocks that exhibit strong ductile deformation have been studied.</p> <p>Bornite and chalcocite are the major copper sulphides. They mainly comprise cement for the clastic grains of the sandstone and suggest a diagenetic origin for their deposition rather than strictly epigenetic formation related to deformation of the host rock. Accessory sulphide minerals include chalcopyrite, covelline, wittichenite, carrolite and cinnabar. They commonly occur as replacement of and/or exsolution from the major Cu sulphides. Alternatively they have been formed through epitactic growth. They are partly formed during later deformation and regional metamorphism.</p> <p>Gold and silver are closely associated the Cu mineralisations. Electrum (AuAg, 3-15 µm) is found in contact with and as inclusions and in cracks in bornite. Additionally, silver occur in amalgam (AgHg), hessite (Ag₂Te), Ag-bearing clausthalite (PbSe), bohdanowiczite (AgBiSe₂), naumannite (Ag₂Se) and unidentified AgBiTe mineral phase often associated native bismuth (Bi) and wittichenite (Cu₃BiS₃). These minerals commonly comprise exsolutions or droplets in the major Cu sulphides and are often enriched at their rims.</p> <p>Platinum most frequently occurs as microscopic grains of sperrylite (PtAs₂) that form clusters of inclusions in bornite and disseminated, interstitial grains in the silicate matrix of the sandstone. Palladium is a minor constituent of some sperrylite, but more commonly comprises complex grains of isomertietite (Pd₁₁Sb₂As₂) and occurs in unidentified PdHgTe and PdBiHg mineral phases which can be Ag-bearing, both in contact with, and separate from the major Cu sulphides.</p>				
Keywords: ore geology	ore mineralogy		copper	
gold	silver		platinum	
palladium				

CONTENTS

1. INTRODUCTION	4
2. LITHOLOGY	5
3. SULPHIDE MINERALS	7
4. NOBLE METALS	15
4.1 Gold.....	15
4.2 Silver	20
4.3 Platinum and palladium.....	23
5. MACROSCOPIC AND MICROSCOPIC DESCRIPTION OF SAMPLES	34
H0810-01 117.5-117.8.....	34
H0810-02 138.0-138.15	35
H0810-03A/B 138.15-138.23	35
H0810-06 135.8-136.0.....	36
H0810-09 136.24-136.36.....	37
H0810-10 136.36-136.48.....	38
H0811-11 139.2-139.5	39
H0811-13 142.5-142.65	40
H0811-14 143.5-143.75	42
H0811-15 144.0-144.1	42
H0811-16 144.1-144.2.....	43
H0814-17A/B 320.45-320.7	44
H0814-19 321.2-321.32	45
H0821-20 127.4-127.6.....	46
6. DISCUSSION	47
7. CONCLUSION	50
8. REFERENCES	51

APPENDIX

Appendix 1: Chemical analyses of core samples from the Nussir copper deposit.

Appendix 2: Chemical composition of minerals based on SEM analyses and normalised to 100 weight%.

1. INTRODUCTION

Core samples have been collected from the four drill holes H0810, H0811, H0814 and H0821 from the eastern part of the Nussir Cu deposit with enrichments of Ag, Au, Pt and Pd. 16 polished thin sections have been prepared and studied. The main aims of the study were to describe the various Cu-sulphide minerals and to identify noble metal-bearing minerals and their relationship to the Cu sulphides. Samples were collected from intervals with various chemical composition (Appendix 1) and varying deformation. Only brief examinations of the host rocks, textures and possible hydrothermal alteration have been carried out.

Important parameters to investigate with respect to the Cu-sulphide minerals and noble-metal minerals include:

- Mineralogy
- Grain size
- Primary - secondary/replacement minerals
- Cement, veins and/or clastic grains
- Relation between mineralogy and lithology/structures
- Relation between the Cu-sulphide minerals and noble-metal minerals

It is important to bear in mind when conducting mineralogical studies aimed at finding noble metal-bearing minerals that the thin sections may not be representative as they only represent minor parts of the analysed core section (5 cm of up to 100 cm). The noble metals can also be 'invisible' by optical microscopy, i.e. forming sub-microscopic ($< 1 \mu\text{m}$) grains or bound in the crystal lattice of sulphide minerals (refractory) and thus not easily detected.

Macroscopic and microscopic descriptions of all the studied samples are given in Section 5, while the major results are presented in the following sections. The optical microscopy were conducted with an Olympus BX60 polarising microscope with 1.5x, 2.5x, 5x, 10x, 40x, and 100x objectives and 10x ocular. The digital photographs were taken with an Axioplan2 imaging microscope. 7 of the polished thin sections have been investigated by use of scanning electron microscope (SEM) in order to verify the very fine-grained minerals of noble metals. The SEM investigations and chemical analyses were performed on a LEO 1450VP electron microscope equipped with Oxford Instruments energy dispersive scanning (EDS) detector (Energy 400 system). The electron beam is generated by a tungsten filament with an accelerating voltage of 15 kV. The diameter of the volume where the elements are electronically activated by the beam is about $10 \mu\text{m}$ for light elements (Al, Si, S) and $1\text{-}1.5 \mu\text{m}$ for heavy elements (Pt, Au, Bi). This means that analyses on mineral grains having a diameter less than the diameter of the beam will incorporate elements from immediately adjacent minerals into the analyses. The analyses performed are semi-quantitative as no standardization procedure has been conducted. The accuracy of the analyses is however in most cases sufficient for mineral identification. The chemical composition of selected minerals based on the SEM analyses is normalised to 100 weight% and is given in Appendix 2.

2. LITHOLOGY

The sedimentary sequence consists generally of layered and laminated fine-grained sandstones and siltstones. Major constituents are sub-angular clastic grains of quartz and feldspar and variable contents of mica (Figure 1). Plagioclase seems to predominate over K-feldspar in most of the studied sections, and biotite is more common than muscovite. Carbonate-rich layers are also found in some of the samples. Identified accessory minerals in addition to sulphides and noble metal-bearing minerals include barite (BaSO_4), rutile (TiO_2), titanite (CaTiSiO_5), tourmaline, monazite ($(\text{Ce,Lu})\text{PO}_4$), zircon, celestine (SrSO_4) and unidentified U-Th phases.

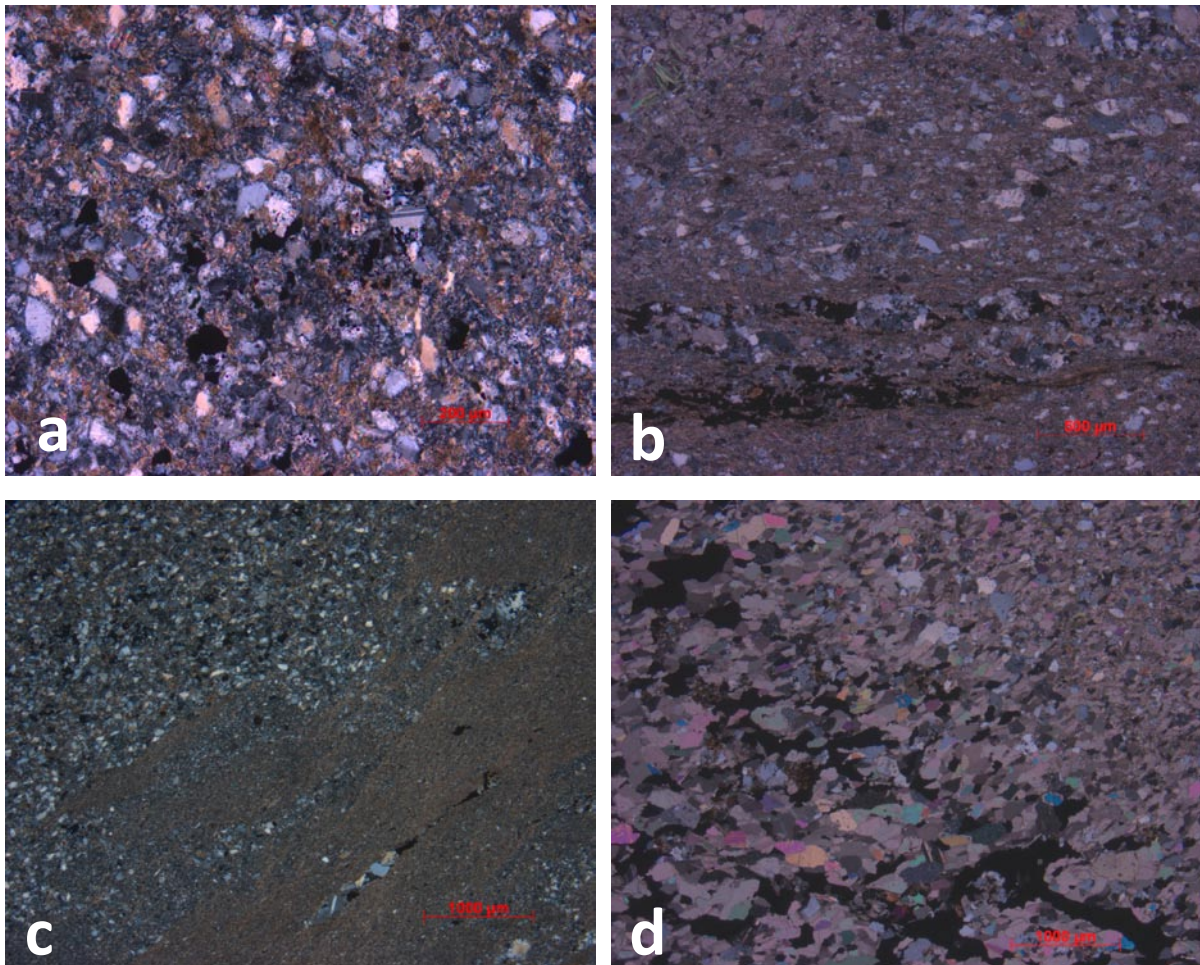


Figure 1: Photomicrographs of typical textures of various sediments. a: Sandstone with unoriented clastic grains of quartz and feldspar (sample H0811-14), b: Sandstone with slightly oriented/foliated clastic grains of quartz and feldspar in a matrix of mica (sample H0810-01), c: Layers and lenses of fine-grained sandstone and mica-rich siltstone (sample H0811-14), d: Fine-grained carbonate-rich layer in sandstone (sample H0814-17A) (transmitted light and crossed polars).

The sedimentary rocks are generally weakly deformed, and have mineral assemblages typical of greenschist-facies metamorphism. Primary layering can be identified in some of the samples, and includes fining-upward sequences. Locally the sedimentary rocks are strongly sheared and folded (e.g. samples H0810-06, H0811-11 (Figure 2) and H0811-14). Note that in sample H0811-13 brittle deformation dominates, and that this sample is collected between the samples H0811-11 and -14 that have experienced strong ductile deformation.

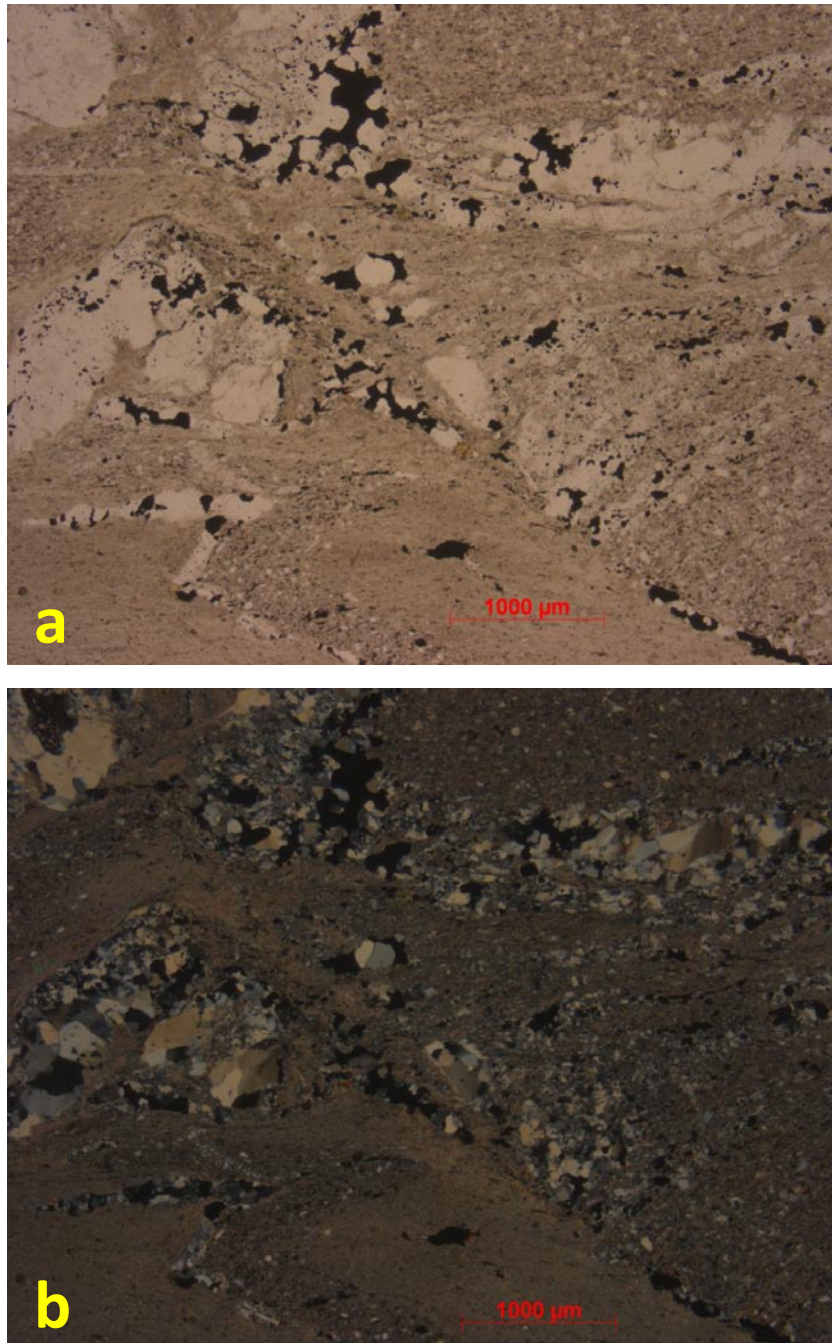


Figure 2: Photomicrographs of strongly sheared fine grained sandstone and siltstone (Sample H0811-11, transmitted light – a: parallel and b: crossed polars).

3. SULPHIDE MINERALS

The major copper-sulphide minerals in the studied samples are bornite (Cu_5FeS_4 - 63.31 % Cu) and chalcocite (Cu_2S - 79.85 % Cu). Chalcopyrite (CuFeS_2 - 34.63 % Cu), and accessory covellite (CuS - 66.46% Cu), occur in minor amounts as secondary replacement along cracks and rims of the major Cu sulphides. Other identified accessory sulphide minerals that most commonly are found in association with the copper-sulphide minerals include wittichenite (Cu_3BiS_3), carrolite ($\text{Cu}(\text{Co},\text{Ni})_2\text{S}_4$), cobaltite (CoAsS) and cinnabar (HgS).

The major Cu sulphides commonly comprise interstitial grains and aggregates forming the matrix for the clastic grains of the sandstone (Figure 3 and Figure 4), and are also found enriched in irregular quartz-rich veinlets and lenses. The common grain size is between 0.1 and 1 mm, and the grain size mostly varies according to the size of the clastic grains. Bornite seems to dominate in most of the sections. Two different coloured types of bornite, brown and purple, are observed in reflected light (in air) under the microscope. SEM analyses indicate no significant compositional differences between them. The purple variety often constitutes composite grains with chalcocite (Figure 5), and myrmekitic intergrowth of these two minerals is also common (Figure 6). Although the evidence is not unequivocal, in many of the samples where bornite and chalcocite comprise composite grains, bornite seems to be replaced by chalcocite (Figure 7).

Chalcopyrite commonly replaces bornite, and comprises tiny single grains in the sedimentary rocks (Figure 8). It occurs most frequently in more highly deformed sedimentary rocks (i.e. in samples H0810-06, H0811-11 and H0811-14) (Figure 9). Several tiny grains of a CuBiS phase that probably represent wittichenite (Cu_3BiS_3) occur as inclusions in and at the rims of bornite and chalcocite in samples H0814-17A/B (Figure 10 and Figure 11), and as inclusions in and at the rim of chalcocite in samples H0821-20 and H0811-16, respectively. The appearance may suggest that wittichenite comprises replacement of major copper sulphides and/or exsolution lamellae along cleavage planes (see also Figure 21 and Figure 22). In the sample H0814-17A/B wittichenite is commonly associated with tiny grains of silver-bearing minerals (see Section 4.2). The average composition of 66 analyses yielded 43,95 % Cu, 33,37 % Bi and 22,67 % S, compared to the stoichiometric composition of 38,45 % Cu, 42,15 % Bi and 19,40 % S for wittichenite (<http://webmineral.com/chemical.shtml>). The higher values of Cu and S in the present analyses are probably due to interference from the neighbouring Cu minerals during these semi-quantitative analyses. Alternatively, the Cu-Bi sulphide may represent another unnamed Cu-Bi sulphosalt.

A few grains (5-30 μm) of assumed cobaltite (CoAsS) occur in sample H0814-17A. They comprise composite grains with bornite and chalcocite. Cobaltite with a tiny inclusion of sperrylite (PtAs_2) is also observed (Figure 27). Carrolite ($\text{Cu}(\text{Co},\text{Ni})_2\text{S}_4$) is found as a tiny grain (15-20 μm) at the rim of bornite in sample H0821-20 (Figure 12). The average of three analyses yields 18,0 % Cu, 35,6 % Co, 3,8 % Ni and 42,6 % S. Cinnabar (HgS) occurs as tiny grains between carbonate grains and grains around chalcopyrite in sample H0814-17B.

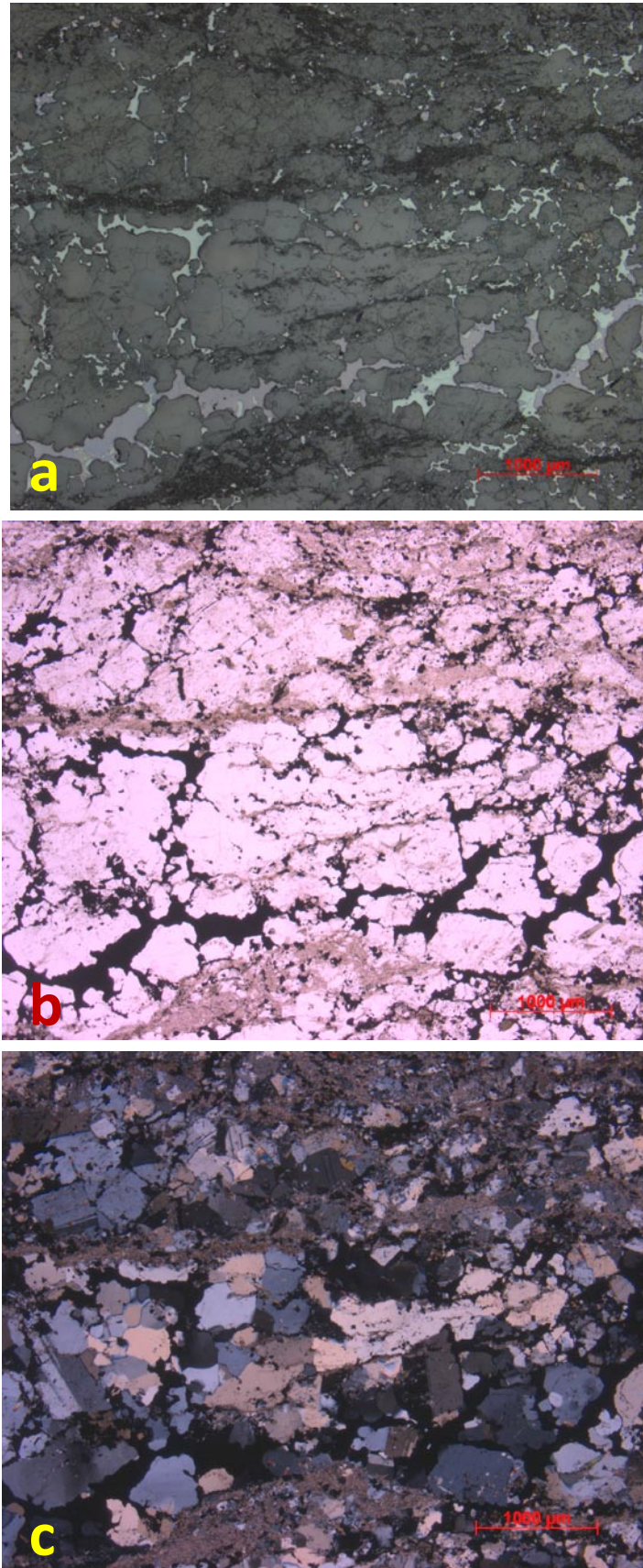


Figure 3: Photomicrographs of typical textures of copper mineralisation in sandstone (sample H0821-20). a: interstitial grains of bornite (purple) and chalcocite (pale blue), as well as partly composite grains of these (reflected light). b and c: same section in transmitted light.

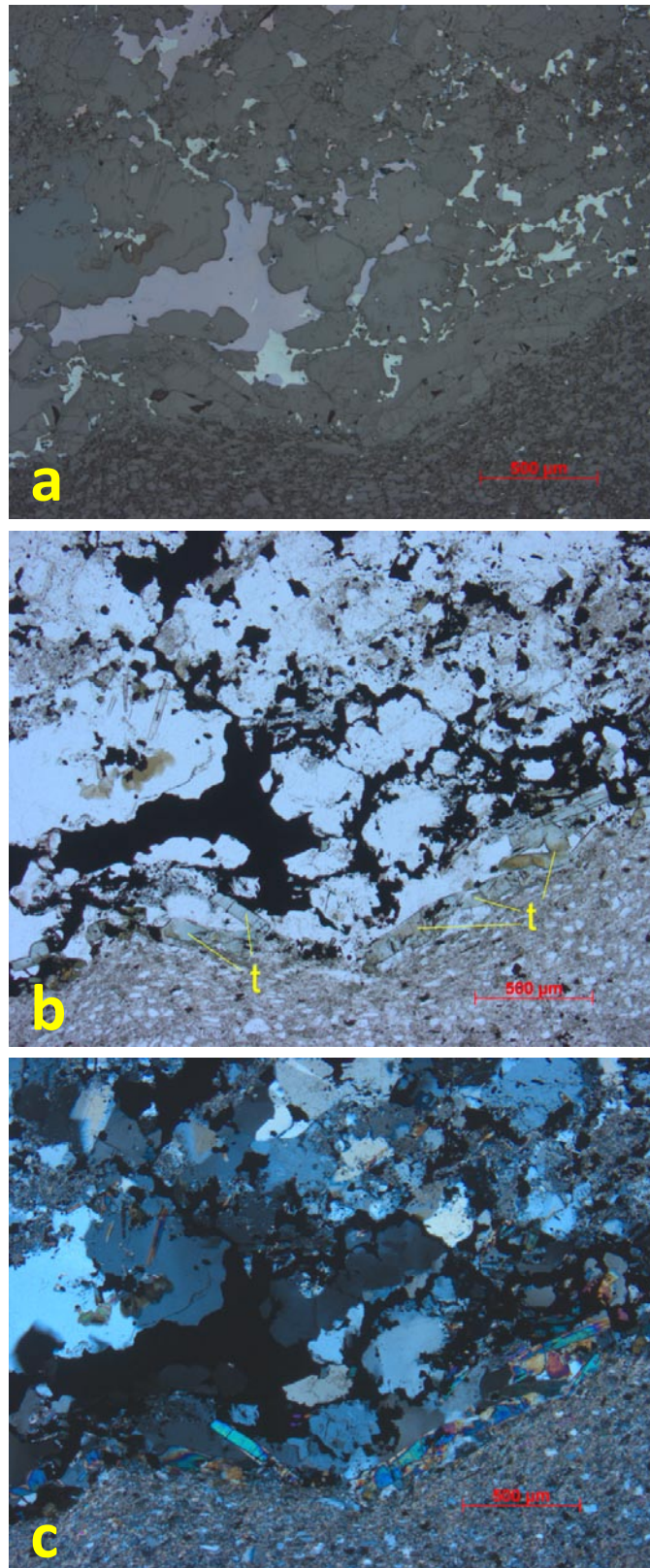


Figure 4: Photomicrographs of typical textures of copper mineralisation in fine-grained sandstone and siltstone (sample H0821-20). a: interstitial grains of bornite (purple) and chalcocite (pale blue) (reflected light). b and c: same section in transmitted light. The tabular grains (greenish blue-brownish) below the Cu sulphides are tourmaline (t) (transmitted light).

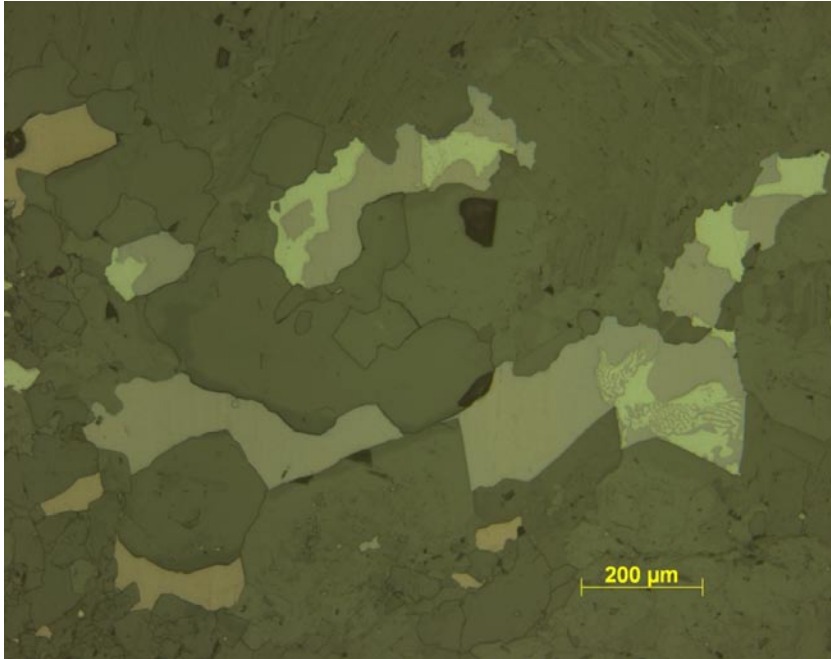


Figure 5: Photomicrograph of composite grains of bornite (purple) and chalcocite (pale blue). Myrmekitic intergrowth of these minerals is seen in the lower right and brown bornite in the upper left corner of the photo (sample H0810-09 - reflected light).

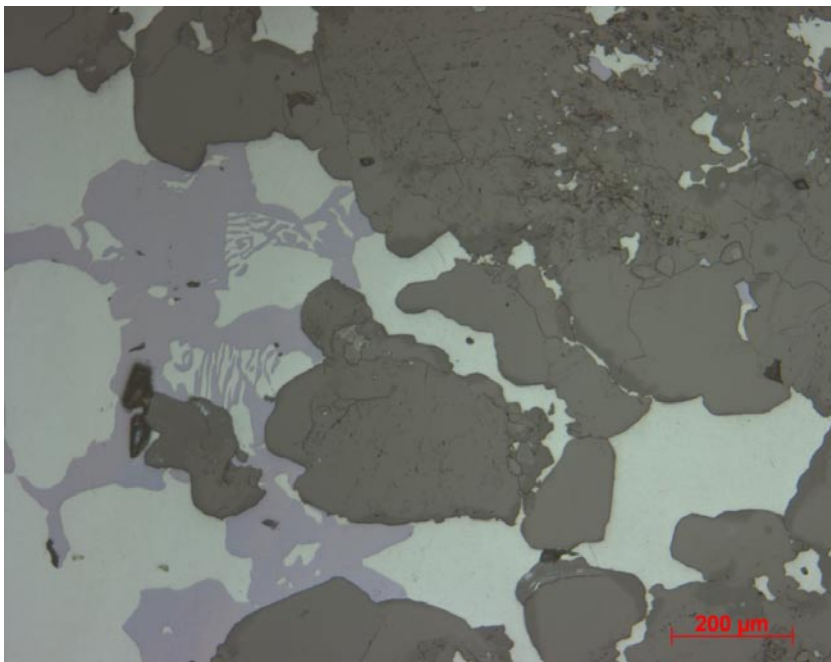


Figure 6: Photomicrograph of myrmekitic intergrowth of bornite (purple) and chalcocite (pale blue) (sample H0821-20 - reflected light).

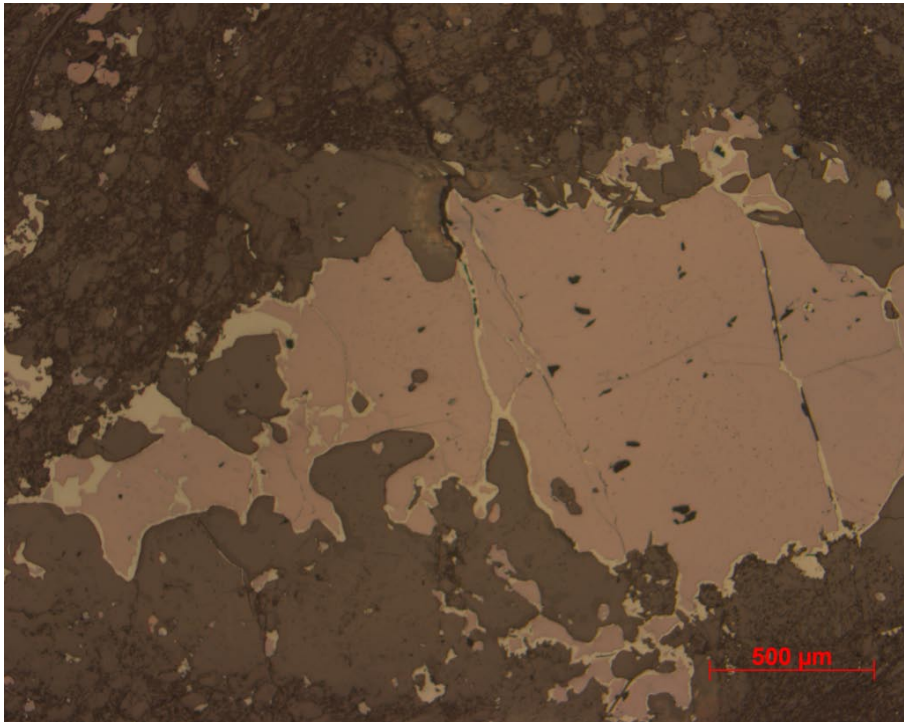


Figure 7: Photomicrograph of bornite (brown) assumed replaced by chalcocite (pale blue) along its rims and intragranular cracks (sample H0810-3 - reflected light).

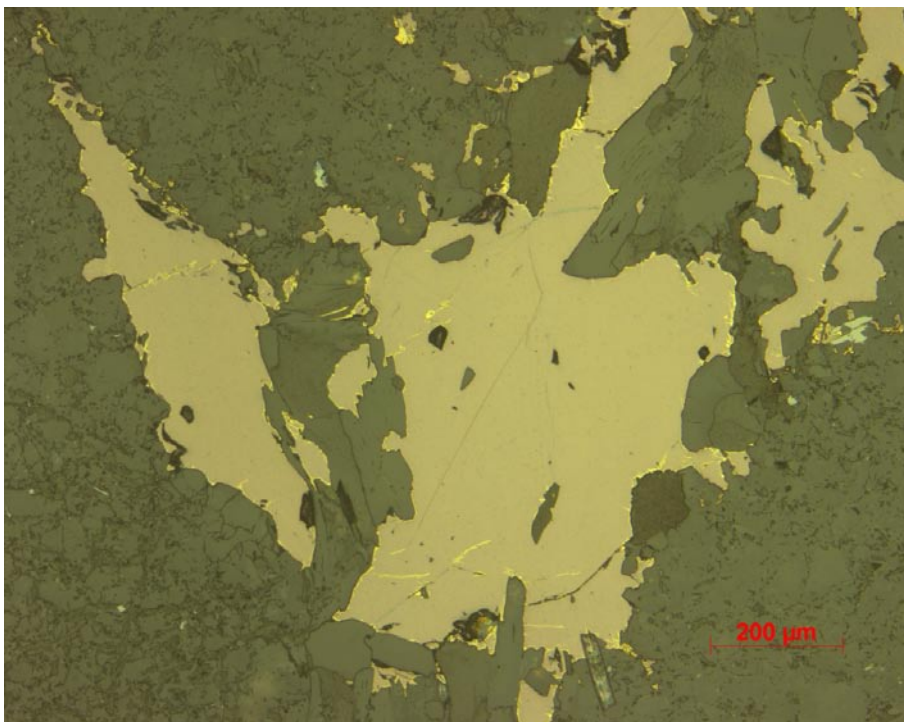


Figure 8: Photomicrograph of bornite (brown) replaced by chalcopyrite (yellow) and covellite (blue crack in upper centre of bornite) (sample H0811-13 - reflected light).

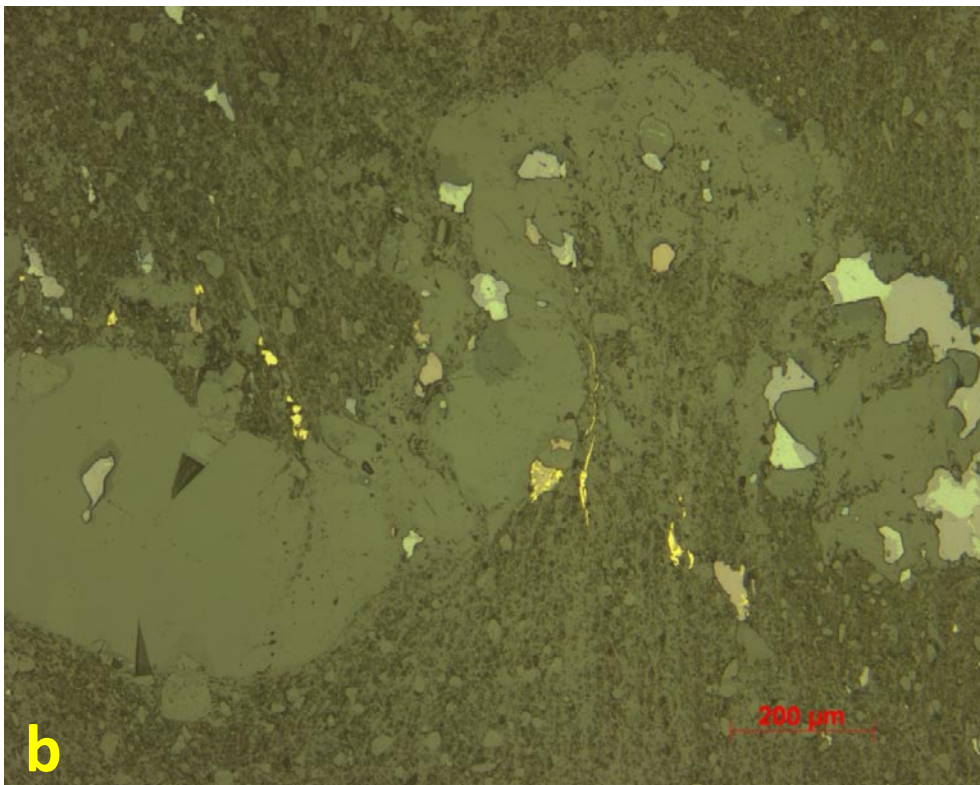
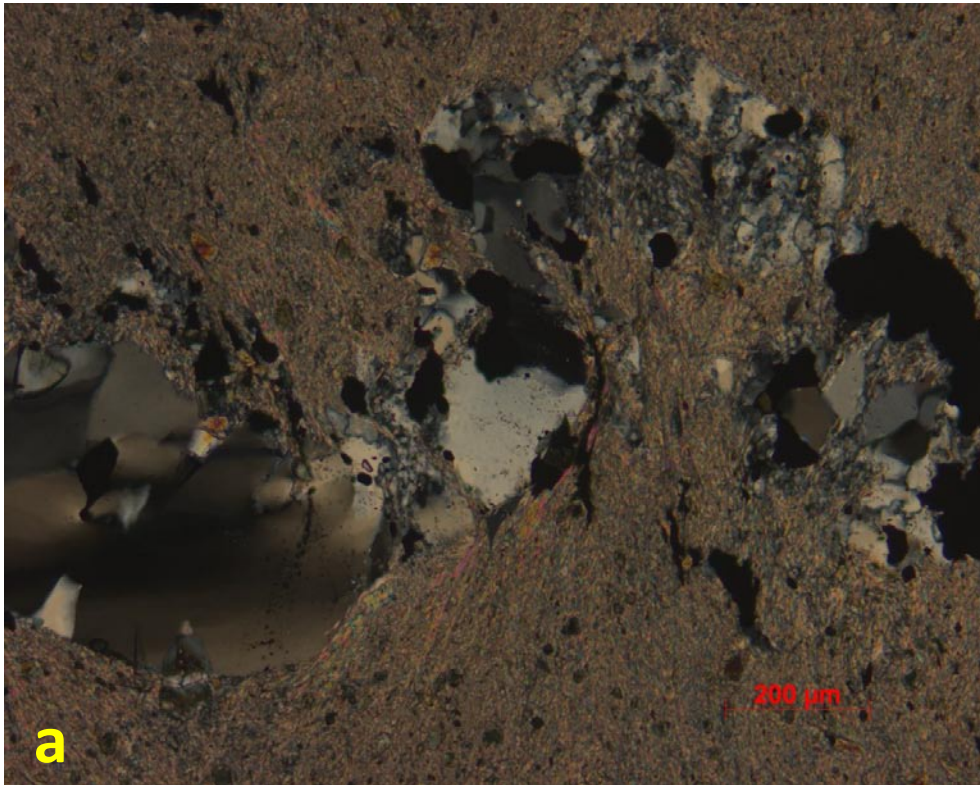


Figure 9: Photomicrographs of folded fine grained sandstone and siltstone with locally elongated grains of chalcopyrite (yellow) oriented along the crenulation cleavage (sample H0811-11, a: transmitted light - crossed polars, b: reflected light).

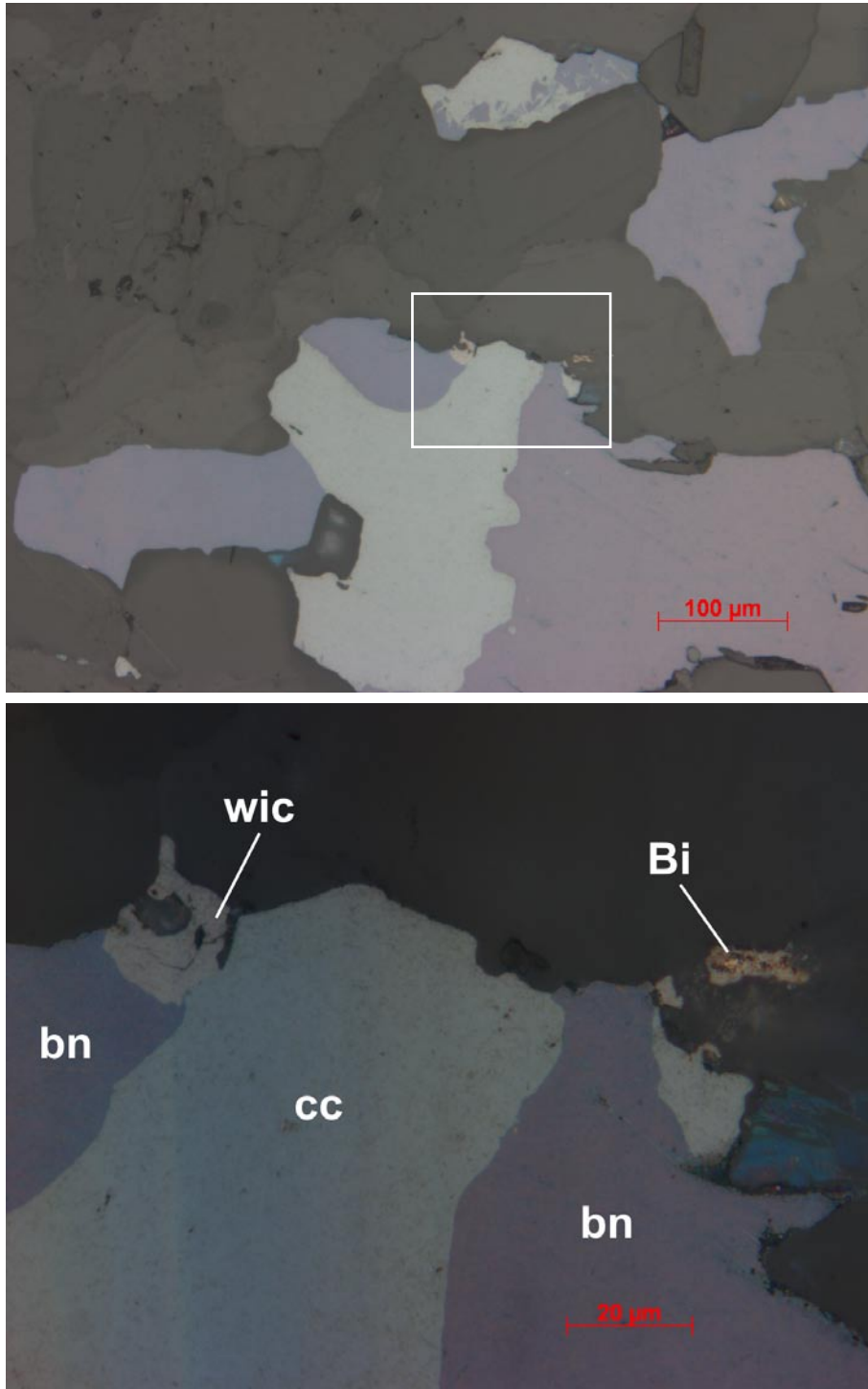


Figure 10: Photomicrographs of wittichenite ($wic - Cu_3BiS_3$) intergrown with bornite (bn) and chalcocite (cc) and gangue minerals in a carbonate layer in sandstone. Wittichenite may replace bornite or formed by epitactic growth. Single grain of native bismuth (Bi) is enclosed by gangue minerals to the right (sample H0814-17A - reflected light).

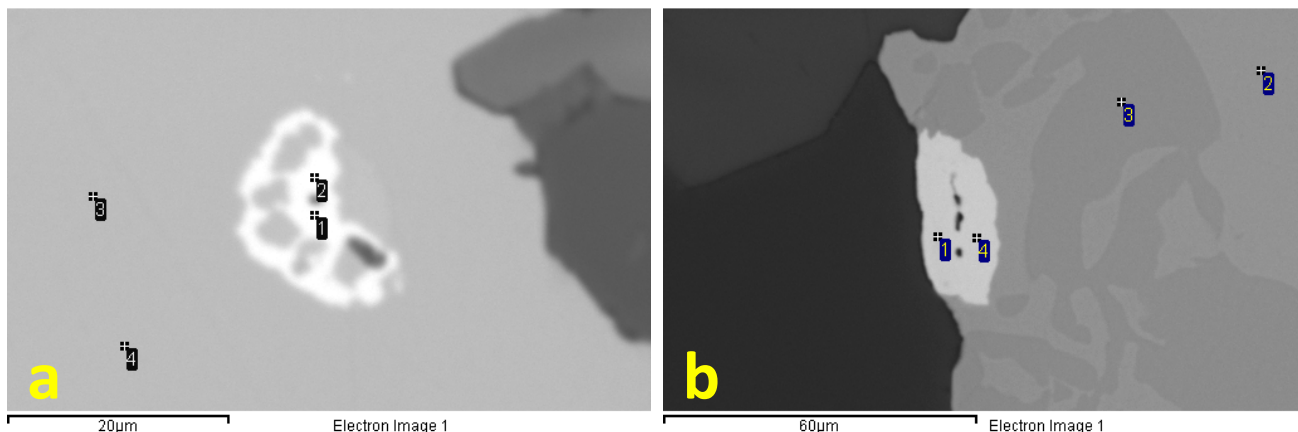


Figure 11: BSEM images showing typical occurrences of wittichenite (Cu_3BiS_3). a: inclusion of wittichenite (1,2) in complex intergrowth with bornite (3,4)(sample H0814-17B). b: wittichenite (1,4) at the boundary between myrmekitic grain of chalcocite (2-light grey) and bornite (3-dark grey) and gangue minerals (sample H0814-17B).

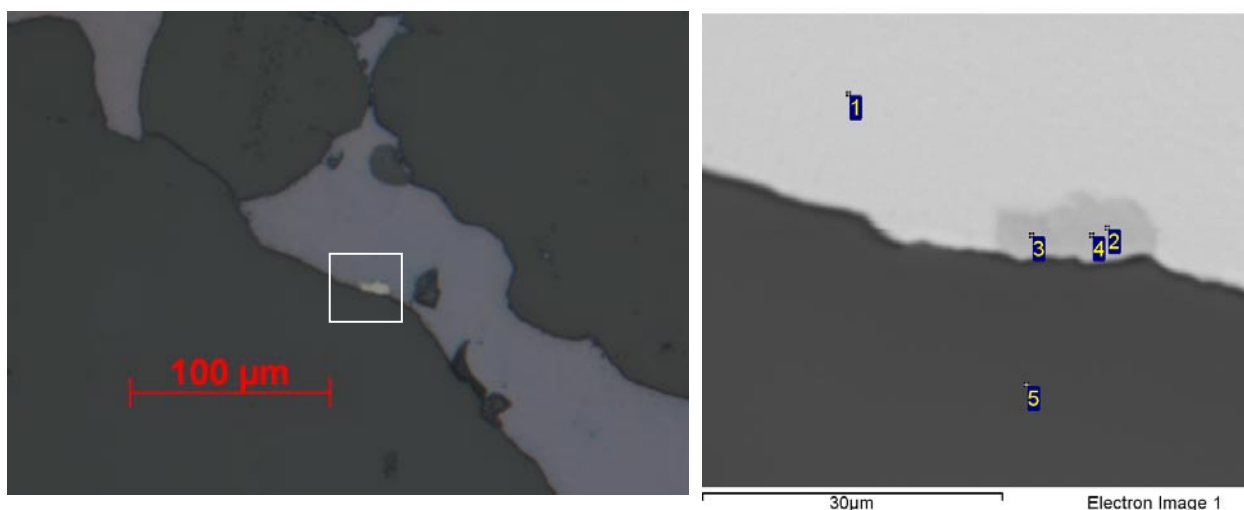


Figure 12: Photomicrograph and BSEM image of carrolite (pale grey, 2-4, $Cu(Co,Ni)_2S_4$) at the grain boundary between bornite (purple, 1) and quartz (5) in sample H0821-20 (reflected light). Numbers refers to analyses in Table 1.

Table 1: SEM analyses normalised to 100 weight% of minerals in Figure 12.

Anal.	Mineral	O	Si	S	Fe	Co	Ni	Cu	Total
(all results in weight%)									
1	Bornite			27.11	11.11			61.77	100.00
2	Carrolite			42.74		35.71	4.56	16.99	100.00
3	Carrolite			42.07		35.12	4.06	18.75	100.00
4	Carrolite			42.85		36.12	2.81	18.22	100.00
5	Quartz	54.93	45.07						100.00

4. NOBLE METALS

4.1 Gold

Gold was identified in a few grains of electrum (AgAu) in samples H0811-13 and H0814-17A and in gold-bearing amalgam in sample H0814-17B. The grain size varies between 3-15 μm , and the Au:Ag ratio in the analysed electrum is from 1:1 to 1:3. Electrum occurs in the carbonate-rich matrix in sample H0814-17A, partly in contact with bornite (Figure 13). However, bornite and/or chalcocite may also contain minor gold in the lattice, but this has not been verified with the present analytical procedure described here.

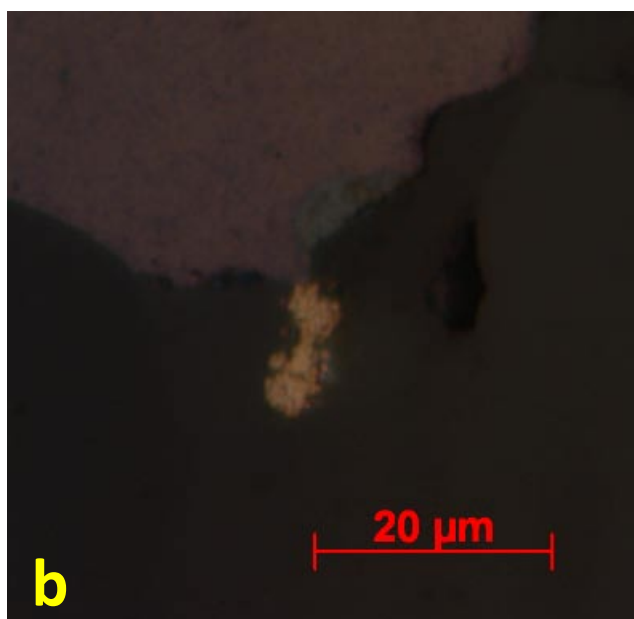


Figure 13 a: Photomicrograph of two interstitial grains of electrum in carbonate-rich sandstone where they occur intergrown with carbonate and bornite. Electrum is in contact with bornite (brown) in the lower centre of the image and composite grain of bornite (purple) and chalcocite (pale blue) to the right. b: Close-up of electrum in contact with bornite in a). The Au:Ag ratio in electrum is 1:3 (sample H0814-17A - reflected light).

Electrum occurs as a tiny inclusion in bornite in fine-grained siltstone (Figure 14, Figure 15) and in crack in bornite in a vein associated with chalcocite in sample H0811-13 (Figure 17). Gold-bearing amalgam is found in sample H0814-17B, but the semi-quantitative analyses do not permit a definite mineral identification (Figure 16).

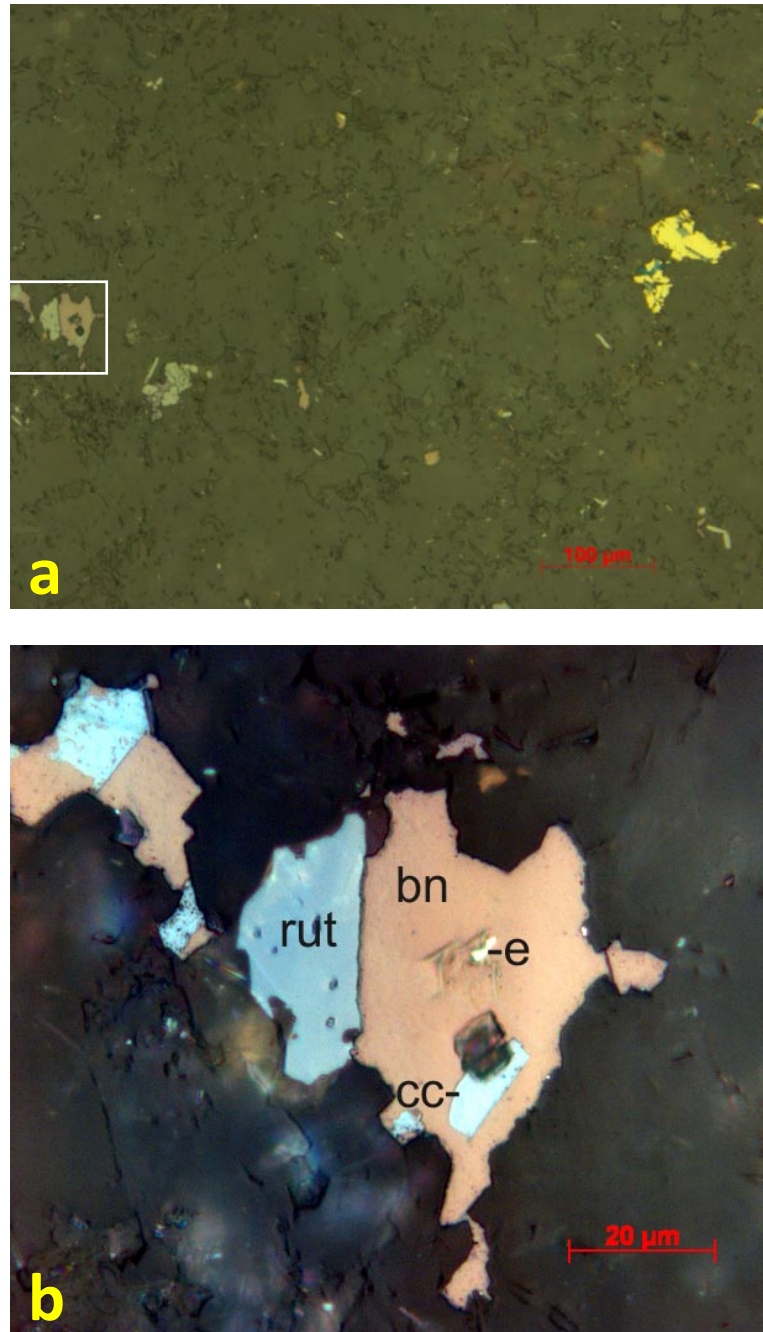


Figure 14a: Electrum is found as a tiny inclusion in bornite (brown) in the middle left of the photomicrograph. Two chalcopyrite grains with lamellae of covelline occur to the right. b: Close-up of the framed area in a) with bornite (bn) containing inclusions of electrum (e) and chalcocite (cc), and in contact with rutile (rut) (sample H0811-13 - reflected light).

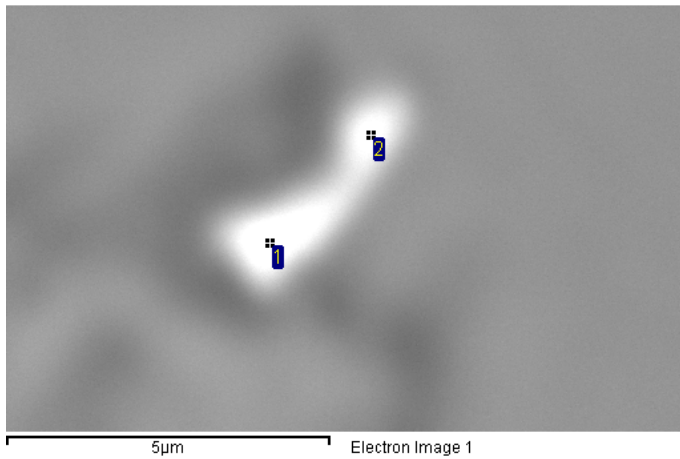


Figure 15: BSEM image of an inclusion of electrum in bornite shown in Figure 14. The weight ratio Au:Ag is around 1:2.

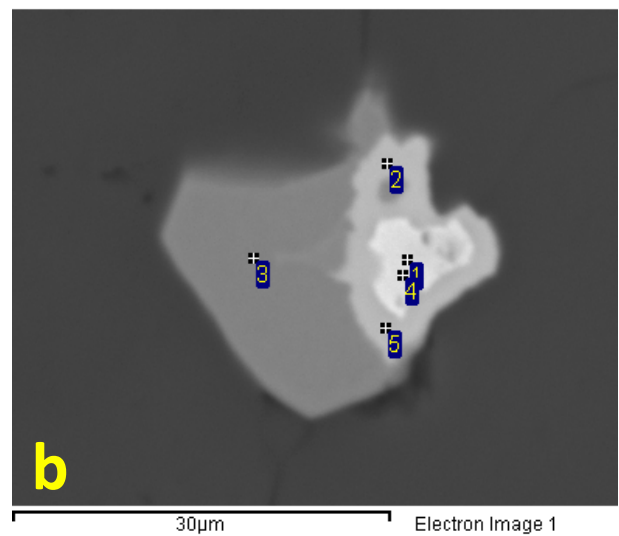
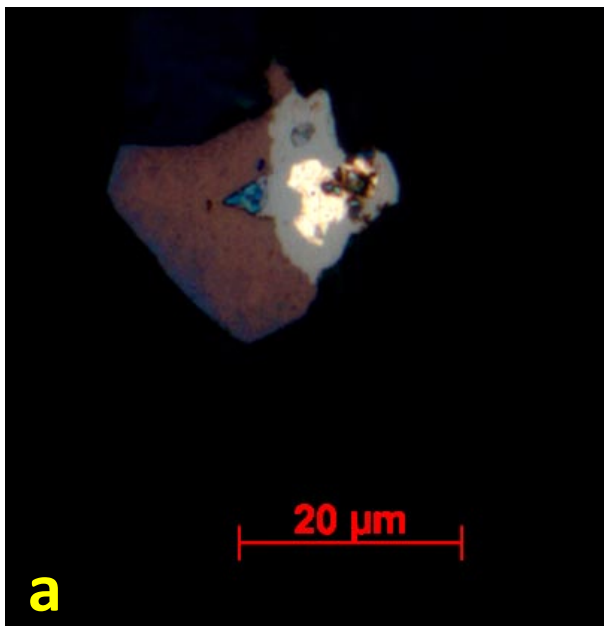


Figure 16a: Photomicrograph of gold-bearing amalgam (yellow) in the core of wittichenite (Cu_3BiS_3 - grey) intergrown with bornite (brown) to the left (sample H0814-17B - reflected light). b: BSEM image of the composite grain in a. Numbers refers to analyses in Table 2.

Table 2: SEM analyses normalised to 100 weight% of minerals in Figure 16.

Anal.	Mineral	S	Fe	Cu	Ag	Au	Hg	Bi	Total
(all results in weight%)									
1	Amalgam				56.01	12.77	31.22		100.00
2	Wittichenite	21.69		44.44				33.86	100.00
3	Bornite	26.48	11.57	61.96					100.00
4	Amalgam				57.36	11.16	31.47		100.00
5	Wittichenite	21.94		44.53				33.53	100.00

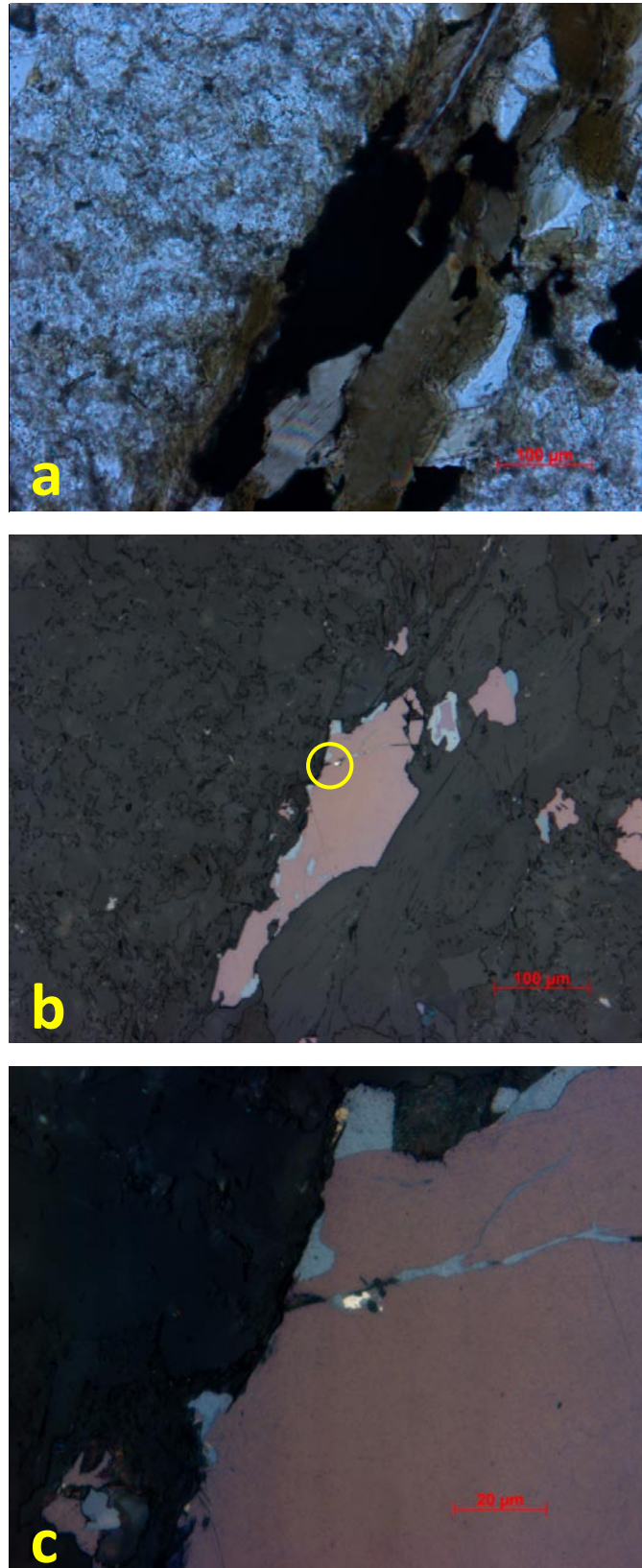


Figure 17: Photomicrographs of a fracture filled with biotite and bornite in fine-grained siltstone. Within the yellow circle there is a micro-fracture filled with electrum, chalcocite and gangue minerals that transects bornite (brown) rimmed by chalcocite (pale blue) (sample H0811-13 - a: transmitted light, b and c: reflected light,).

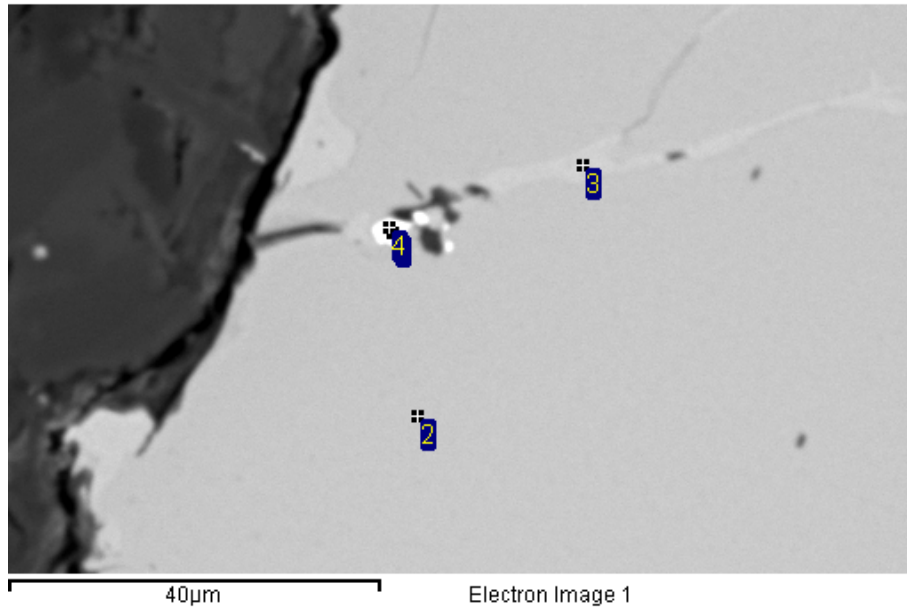


Figure 18: BSEM image of electrum (1 and 4) and chalcocite (3) in crack in bornite (2) as shown in Figure 17. Numbers refers to analyses below. The Au:Ag ratio is around 1:1 (sample H0811-13). Numbers refers to analyses in Table 3.

Table 3: SEM analyses normalised to 100 weight% of minerals in Figure 18.

Anal.	Mineral	S	Fe	Cu	Ag	Au	Total
(all results in weight%)							
1	Electrum				46.40	53.60	100.00
2	Bornite	29.37	10.58	60.05			100.00
3	Chalcocite	26.59	2.35	71.07			100.00
4	Electrum				50.46	49.54	100.00

4.2 Silver

Silver (Ag) has been identified in electrum (AgAu, see above), amalgam (AgHg), gold-bearing amalgam ((Au,Ag)Hg) and hessite (Ag₂Te). The Ag:Hg weight ratio is around 2:1 in amalgam (Figure 19 and Figure 20). In addition silver occurs in mineral phases suggested to represent bohdanowiczite (AgBiSe₂) and naumannite (Ag₂Se), and in an unidentified AgBiTe mineral phase often associated with clausthalite (PbSe), native bismuth (Bi) and wittichenite (Cu₃BiS₃). Clausthalite may contain up to ~8% Ag. Unidentified palladium-bearing mineral phases can also be Ag-bearing (see section 4.3). Hessite (Ag₂Te) was identified in the samples H0811-15 and H0814-17A, while the other Ag-bearing minerals occur in the samples H0814-17A/B.

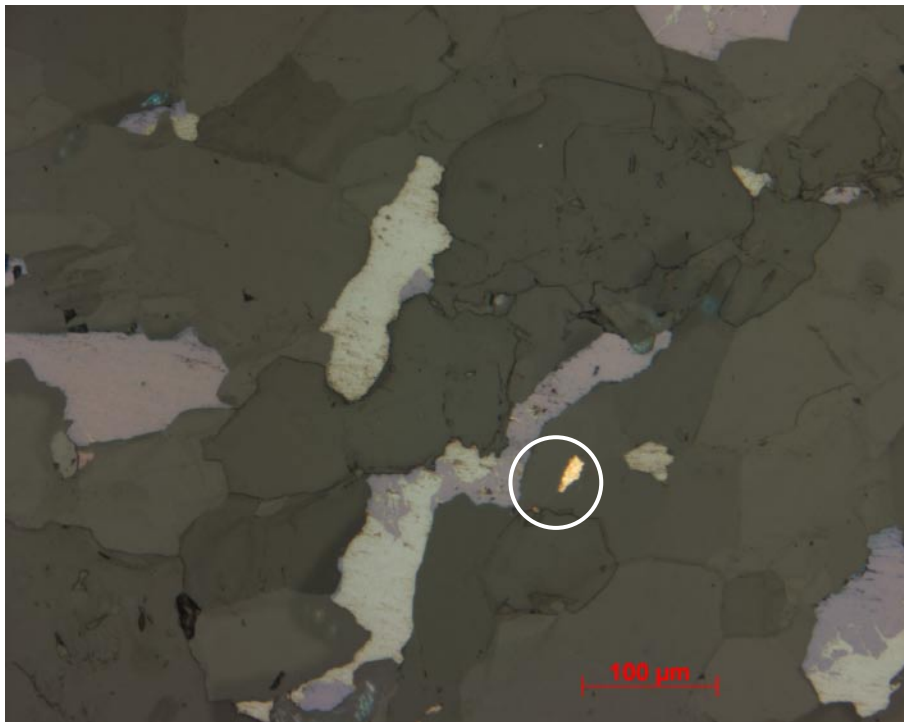


Figure 19: Photomicrograph of single grain of amalgam (AgHg) (pale yellow) in a matrix of carbonate sandstone, that also contains composite grains of bornite (purple) and chalcocite (pale blue) and bornite (brown; centre left) (sample H0814-17B - reflected light).

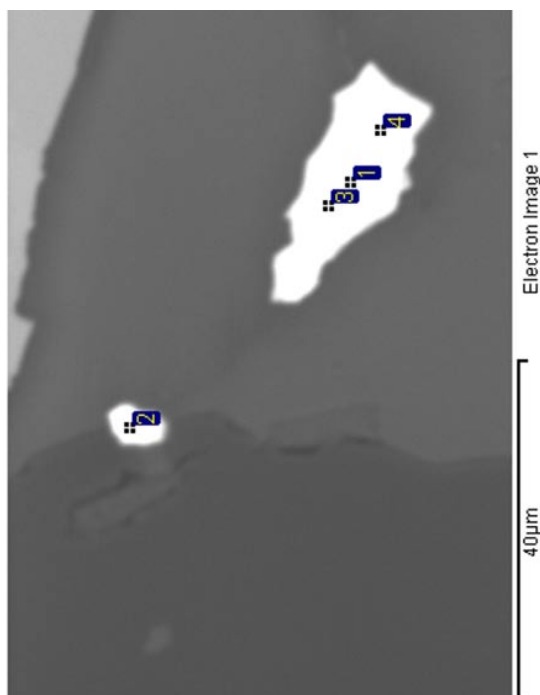


Figure 20: BSEM image of amalgam intergrown with calcite shown within the circle in Figure 19. The Ag:Hg ratio is around 2:1. The tiny grain below consists of native bismuth (Bi) and occurs at the boundary between calcite (grey) and plagioclase (dark grey).

The silver-bearing minerals appear to be clearly associated with the major Cu-sulphide minerals, dominantly bornite. The complex mineralogy of these can be demonstrated in several cases. Typical occurrences of Ag-bearing minerals at the margin of and as inclusions in bornite are shown in Figure 21 and Figure 22. They may be formed as replacement of bornite, as exsolution lamellae or through epitaxial growth.

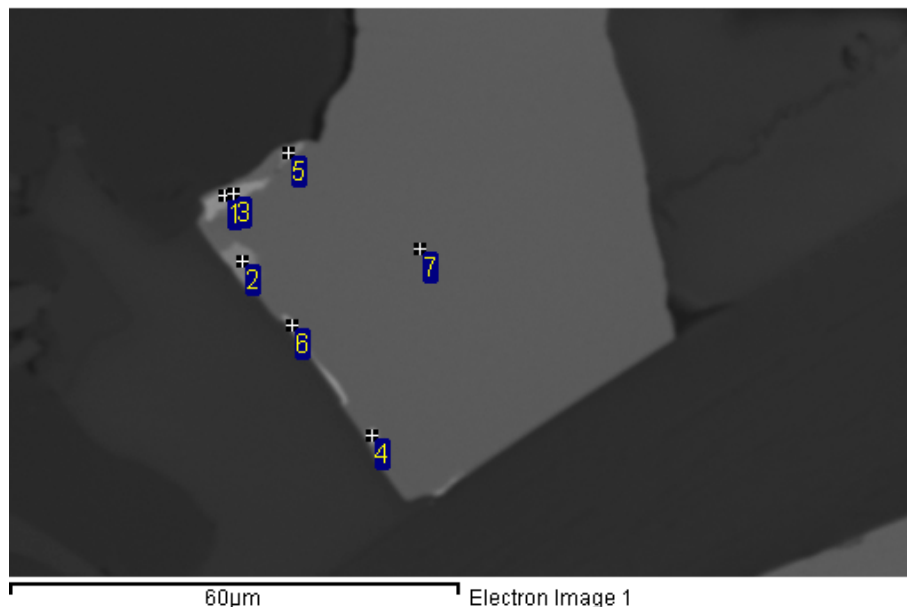


Figure 21: BSEM image of bornite (7) with bohdanowiczite (1,3 – AgBiSe_2), Ag-bearing clausenthalite (4,6 – PbSe), naumannite (Ag_2Se) (5) and wittichenite (2 – Cu_3BiS_3) at its margin (sample H0814-17B). Numbers refers to analyses in Table 4.

Table 4: SEM analyses normalised to 100 weight% of minerals in Figure 21.

Anal.	Mineral	S	Fe	Cu	Se	Ag	Pb	Bi	Total
(all results in weight%)									
1	Bohdanowiczite				32.93	25.36		41.71	100.00
2	Wittichenite	23.04		40.21				36.75	100.00
3	Bohdanowiczite				34.11	23.80		42.10	100.00
4	Clausenthalite				22.42	3.04	74.54		100.00
5	Naumannite				25.74	74.26			100.00
6	Clausenthalite				22.51	4.25	73.24		100.00
7	Bornite	28.74	12.17	59.09					100.00

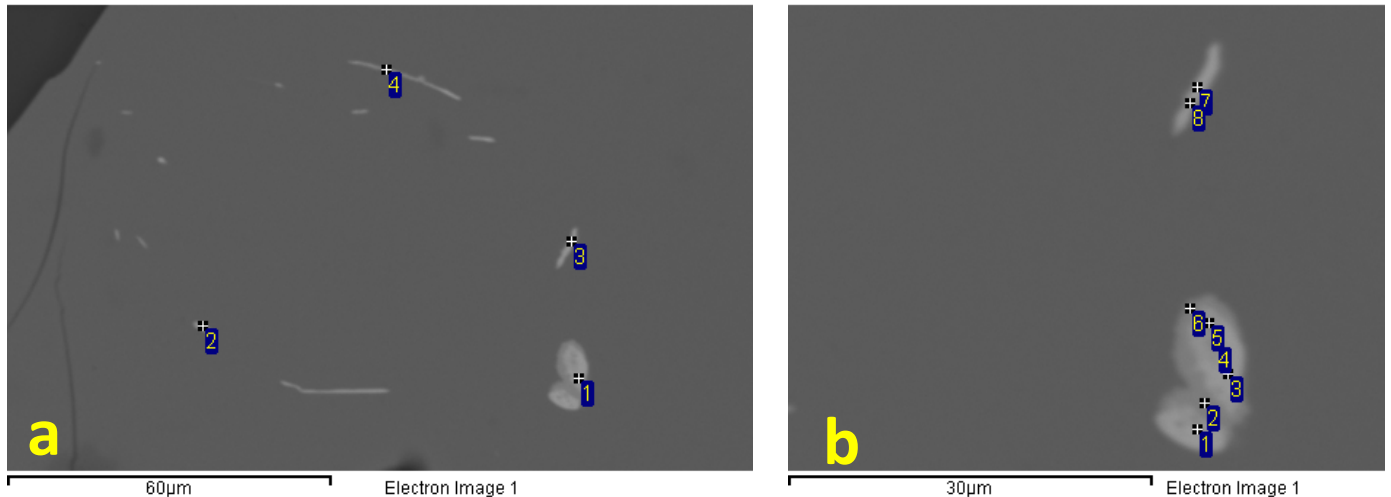


Figure 22: BSEM images of mineral inclusions in bornite where b) is a close-up of the lower right corner of a). The complex mineralogy is clearly demonstrated in the major inclusion in b). It is zoned and comprises a core of Ag-bearing clausthalite (1,3 – PbSe), enclosed by bohdanowiczite (4,5 – AgBiSe₂) and wittichenite in the outer rim (2,6 – Cu₃BiS₃). The upper grain to the right is clausthalite (7,8 – PbSe). Numbers refers to analyses in Table 5 for a) and Table 6 for b) (sample H0814-17B).

Table 5: SEM analyses normalised to 100 weight% of minerals in Figure 22a.

Anal.	Mineral	S	Fe	Cu	Se	Ag	Pb	Total
(all results in weight%)								
1	Clausthalite				25.20	3.09	71.71	100.00
2	Clausthalite				27.67		72.33	100.00
3	Clausthalite				22.68		77.32	100.00
4	Bornite + ?	27.74	9.76	54.19	8.31			100.00

Table 6: SEM analyses normalised to 100 weight% of minerals in Figure 22b.

Anal.	Mineral	S	Cu	Se	Ag	Pb	Bi	Total
(all results in weight%)								
1	Clausthalite			28.35	7.93	63.72		100.00
2	Wittichenite	23.09	43.16				33.75	100.00
3	Clausthalite			26.13	4.09	69.78		100.00
4	Bohdanowiczite			37.43	15.97		46.60	100.00
5	Bohdanowiczite			35.18	20.17		44.65	100.00
6	Wittichenite	24.75	46.72				28.54	100.00
7	Clausthalite			22.91		77.09		100.00
8	Clausthalite			23.34		76.66		100.00

4.3 Platinum and palladium

Platinum (Pt) occurs mainly concentrated in sample H0811-15 where it most frequently forms microscopic grains of sperrylite (PtAs_2). A few grains of sperrylite containing minor amounts of palladium (Pd) are also identified in the samples H0814-17A/B. Palladium is also found in sample H0814-17B where it occurs concentrated in a few SbAs-bearing grains (4-8 μm) that probably represent isomertieite ($\text{Pd}_{11}\text{Sb}_2\text{As}_2$), and in sample H0814-17A as unidentified PdHgTe and PdBiHg mineral phases which can be Ag-bearing and occur in association with hessite (Ag_2Te) and an unidentified AgBiTe mineral.

Sperrylite in sample H0811-15 occurs both as inclusions in the major Cu-sulphide minerals, dominantly bornite, and disseminated, interstitial grains in the silicate matrix of the sandstone without any contact to the Cu-sulphide minerals (Figure 23). Locally, the tiny grains of sperrylite (PtAs_2) are concentrated and form clusters of inclusions in bornite and silicate (e.g. K-feldspar) as shown in Figure 25.

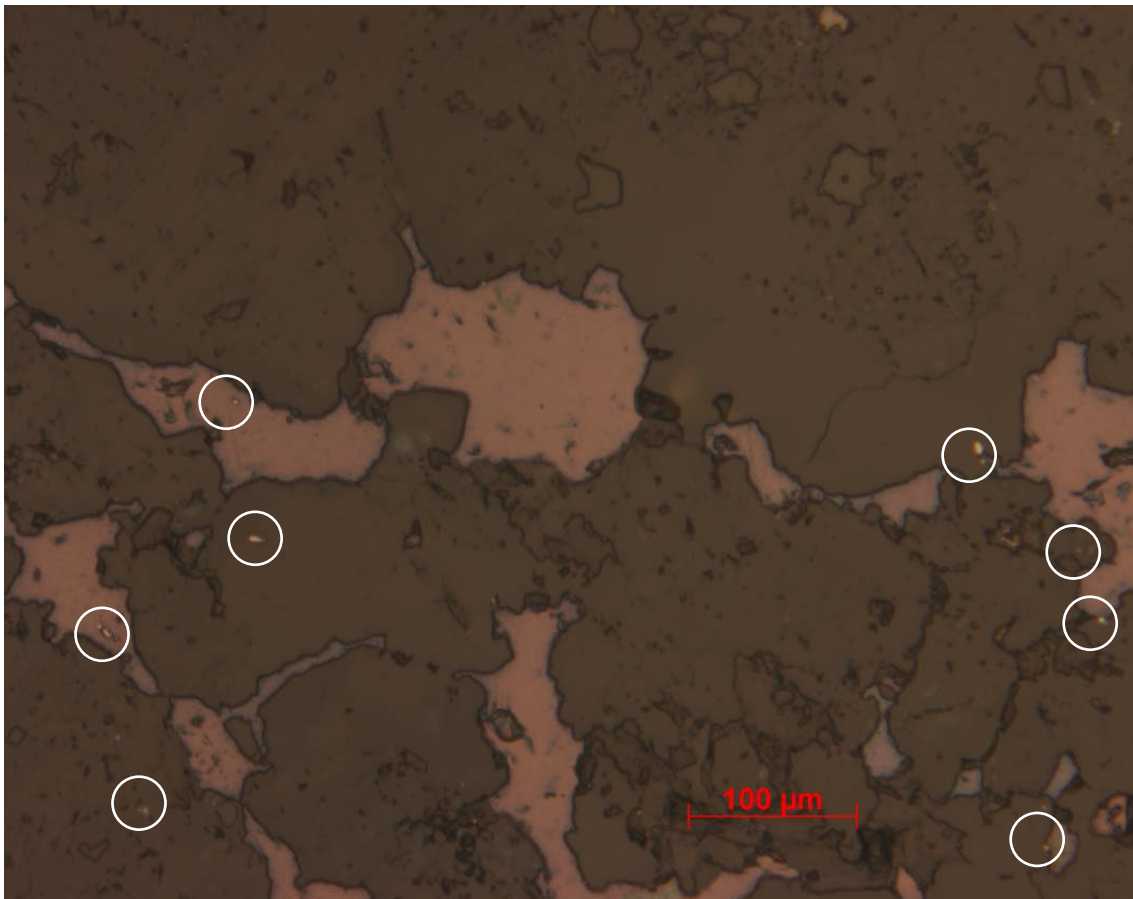


Figure 23: Photomicrograph showing the distribution of several tiny grains of sperrylite (PtAs_2) as inclusions in bornite (brown) and in the silicates dominated by quartz and K-feldspar (dark brown) in sample H0811-15 (reflected light).

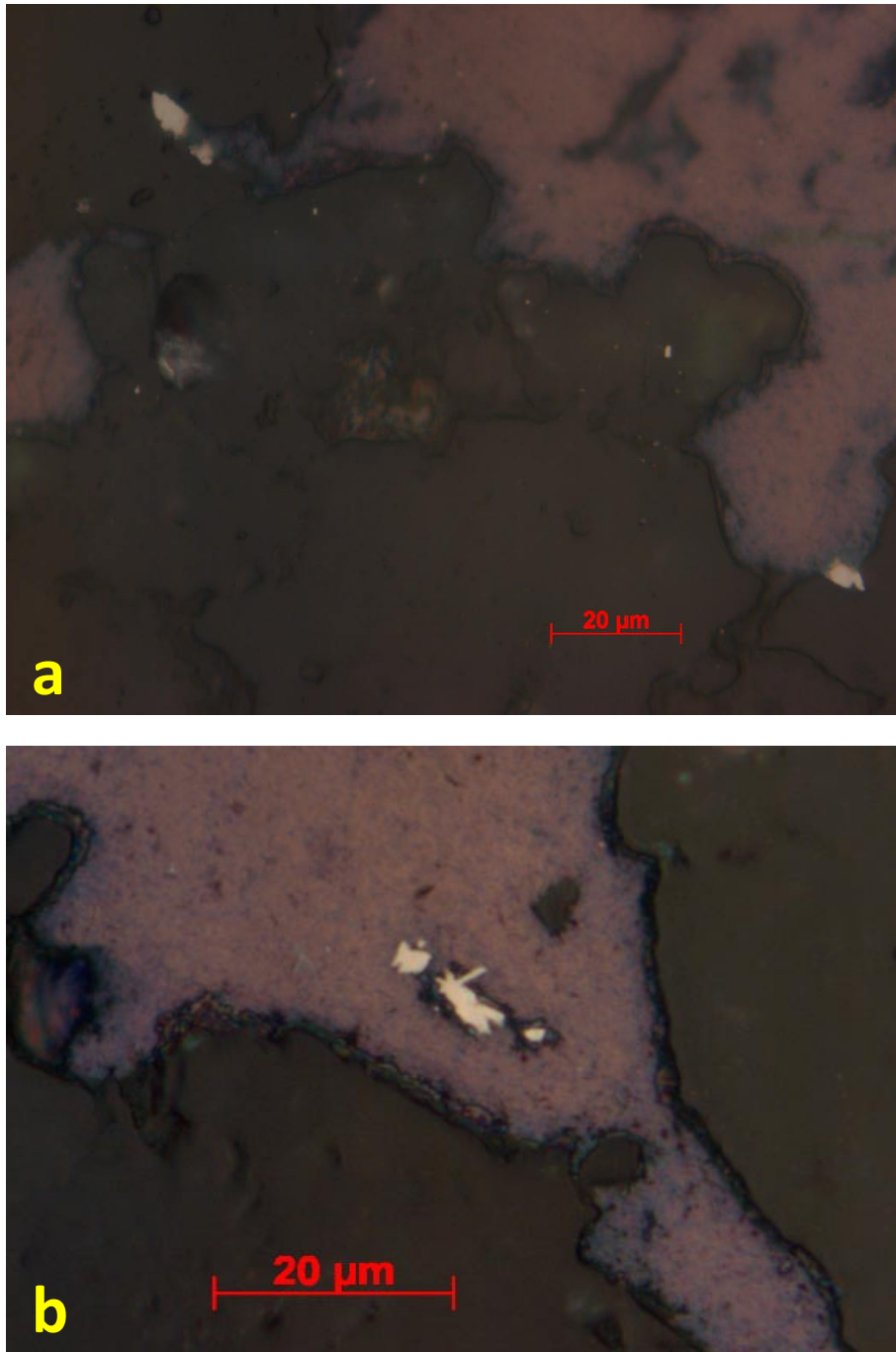


Figure 24: Close-up photomicrographs of sperrylite, bornite and silicate minerals in Figure 23. a: from the right side of Figure 23. Note that all of the very tiny bright grains represent sperrylite. b: sperrylite inclusions in bornite from the left side of Figure 23 (reflected light). Representative analyses of sperrylite and bornite are shown in Table 7.

Table 7: SEM analyses normalised to 100 weight% of sperrylite and bornite in Figure 24b.

Anal.	Mineral	S	Fe	Cu	As	Pt	Total
(all results in weight%)							
1	Sperrylite				42.05	57.95	100.00
2	Sperrylite				43.84	56.16	100.00
3	Bornite	29.10	11.10	59.80			100.00

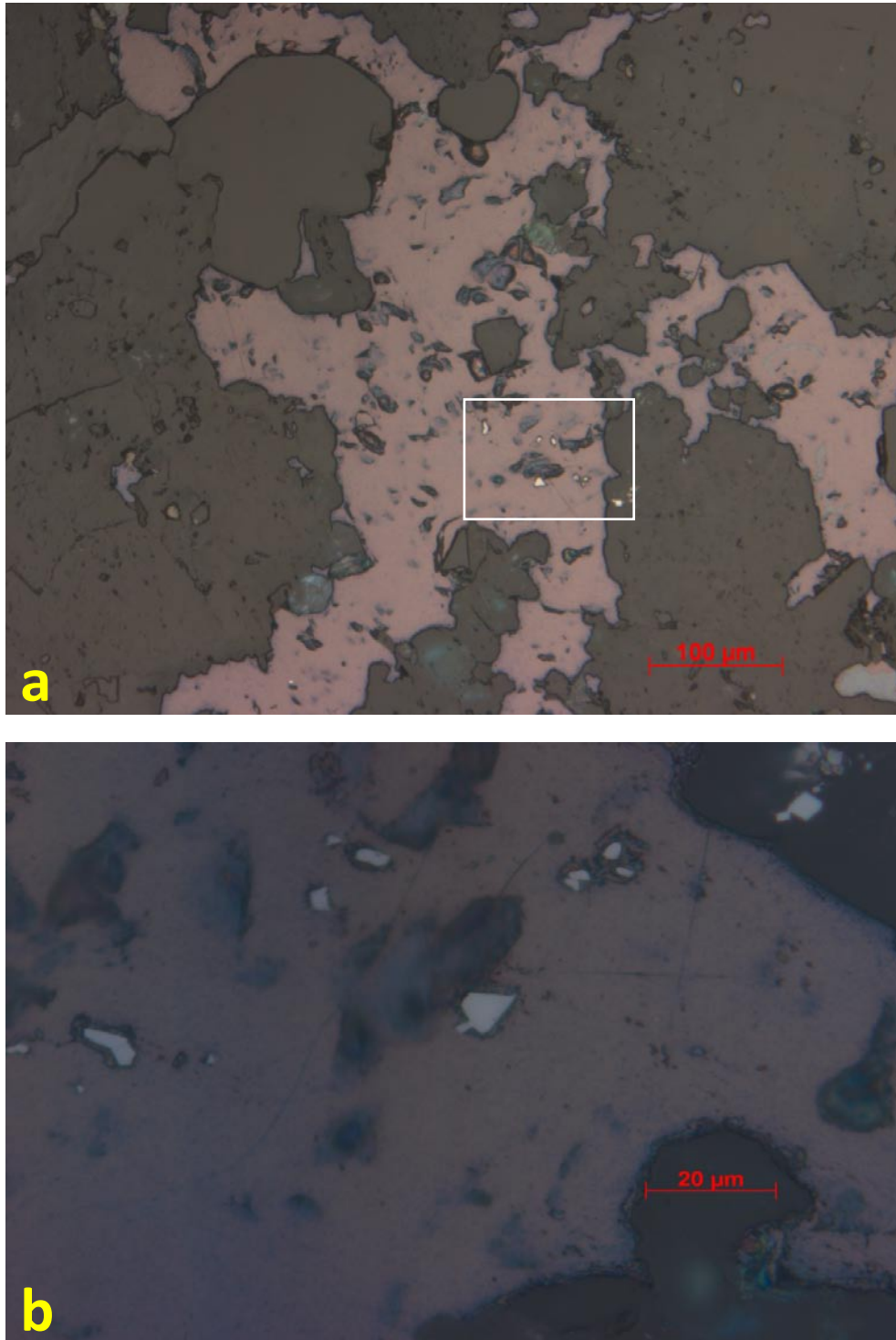


Figure 25a: Photomicrographs of several microscopic grains of sperrylite (white - PtAs_2) in bornite (brown). b: Close-up of the framed area in a) (sample H0811-15 - reflected light).

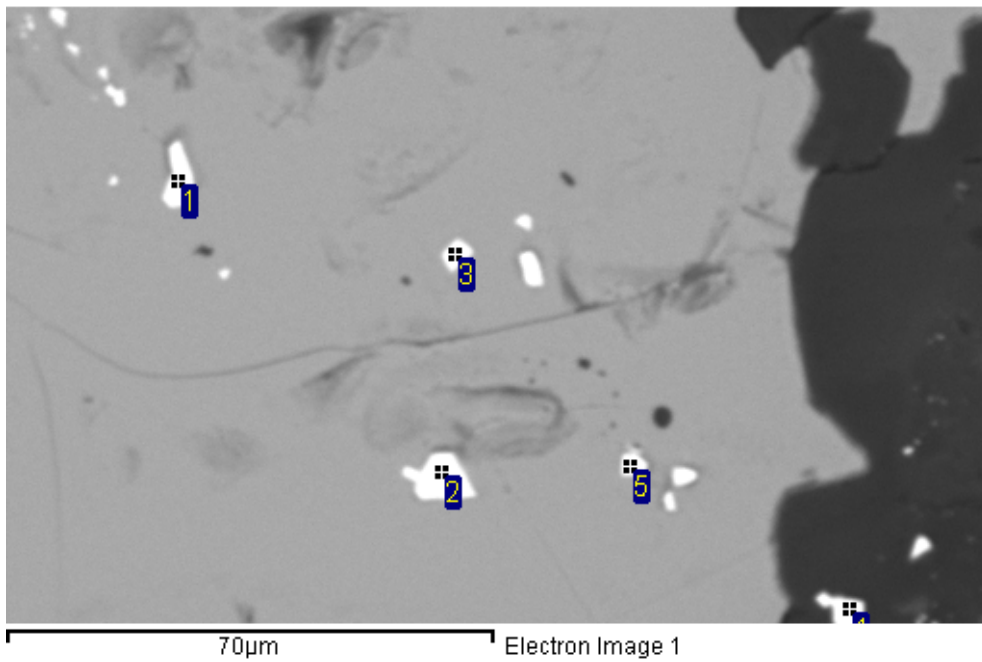


Figure 26: BSEM image of sperrylite (1-5) in bornite from the sample in Figure 25. Numbers refers to analyses in Table 8 (sample H0811-15).

Table 8: SEM analyses normalised to 100 weight% of sperrylite in Figure 26.

Anal.	Mineral	As	Pt	Total
(all results in weight%)				
1	Sperrylite	42.10	57.90	100.00
2	Sperrylite	42.51	57.49	100.00
3	Sperrylite	42.58	57.42	100.00
4	Sperrylite	44.11	55.89	100.00
5	Sperrylite	43.22	56.78	100.00

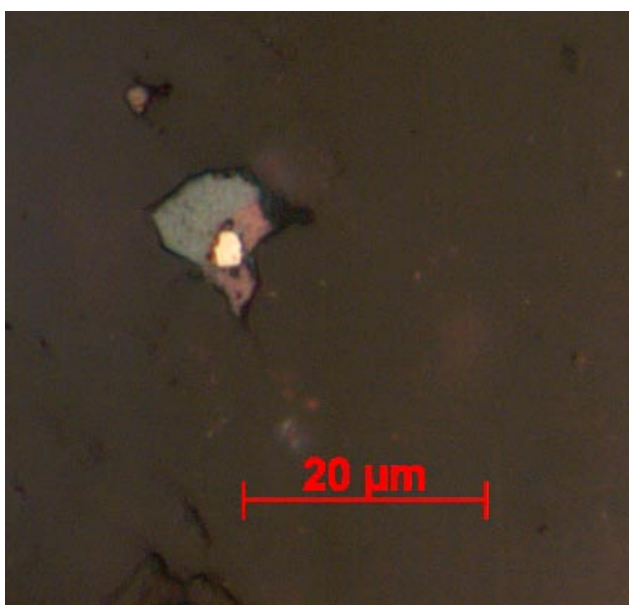


Figure 27: Photomicrograph of composite grain of chalcocite (pale blue) and bornite (brown) with inclusion of cobaltite (CoAsS - bright yellow). A very tiny inclusion of sperrylite ($PtAs_2$) occurring in cobaltite is hardly visible, but was verified by use of SEM (Figure 28) (sample H0811-15 – reflected light).

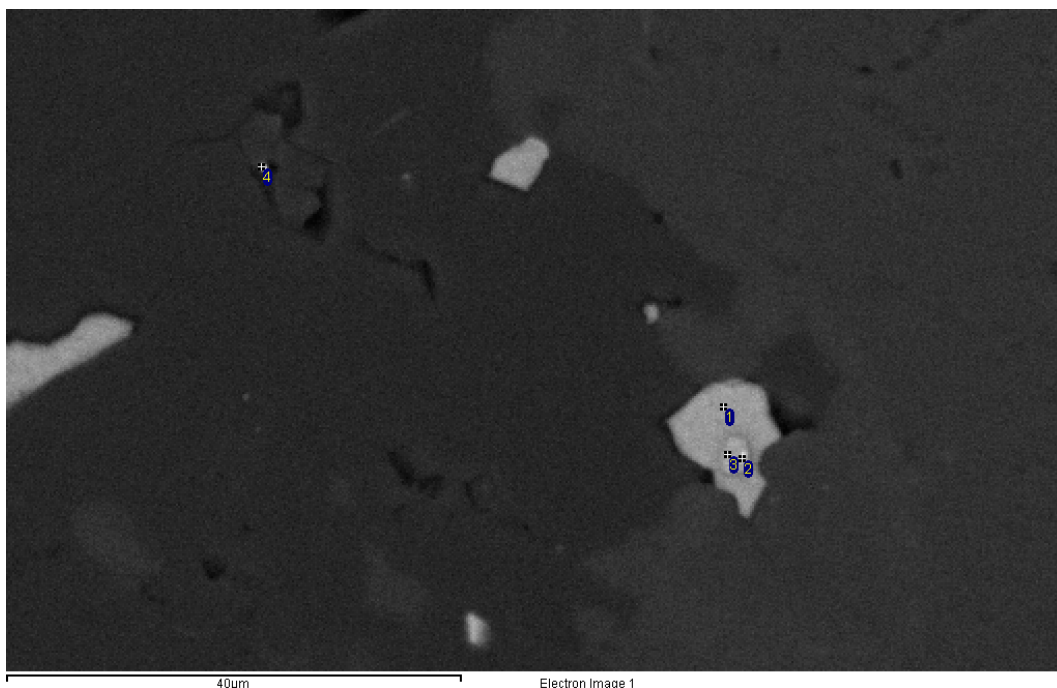


Figure 28: BSEM image of the composite grain in Figure 27 of chalcocite (1) and bornite with inclusion of cobaltite (3 - CoAsS) with a very tiny inclusion of sperrylite (2 - PtAs_2). Note the very tiny grain of sperrylite (4) interstitial the silicates. Numbers refers to analyses in Table 9 (sample H0811-15).

Table 9: SEM analyses normalised to 100 weight% of minerals in Figure 28. Note the interference from cobaltite in the analysis of sperrylite.

Anal.	Mineral	S	Fe	Co	Cu	As	Pt	Total
(all results in weight%)								
1	Chalcocite	28.23			71.77			100.00
2	Sperrylite/cobal.	22.88	3.17	17.70	17.68	28.86	9.72	100.00
3	Cobaltite	29.21		30.61	3.06	37.12		100.00
4	Sperrylite					39.93	60.07	100.00

The PGE mineralogy in sample H0811-15 is simple and only sperrylite (PtAs_2) has been identified, whereas in the samples H0814-17A/B it is more complex. Palladium (Pd) is enriched in these samples where even sperrylite is Pd-bearing (Figure 29). The highest Pd content of the cores is recorded in the interval where these samples have been collected (Appendix 1). The PGE minerals both occur associated with the Cu-sulphide minerals and as separate grains in the carbonate-rich sedimentary rock.

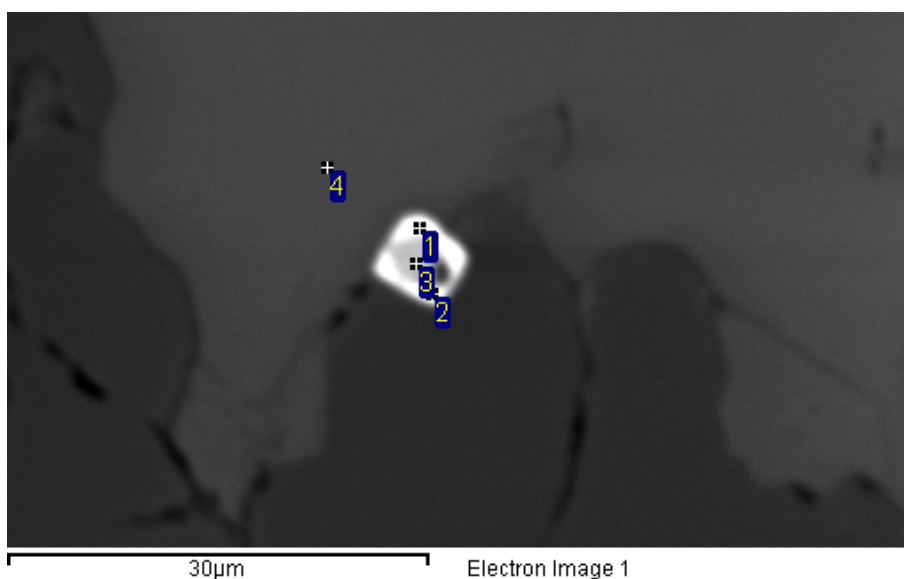


Figure 29: BSEM image of sperrylite (1-2) enveloping chalcocite (3) at the contact between calcite (4 - CaCO_3) and quartz (dark grey) in sample H0814-17A. Numbers refers to analyses in Table 10.

Table 10: SEM analyses normalised to 100 weight% of minerals in Figure 29.

Anal.	Mineral	C	O	S	Ca	Cu	As	Pd	Pt	Total
(all results in weight%)										
1	Sperrylite						44.92		55.08	100.00
2	Sperrylite						43.77	3.87	52.36	100.00
3	Chalcocite			20.16		79.84				100.00
4	Calcite	14.14	55.73		30.13					100.00

More complex grains of PGE-bearing minerals are shown in Figure 30 and Figure 31. Sperrylite (PtAs_2) and isomertieite ($\text{Pd}_{11}\text{Sb}_2\text{As}_2$) are accompanied by some mineral phases that are not clearly identified with the present analytical procedure. Associated metals in these are to varying amounts silver (Ag), bismuth (Bi) and mercury (Hg) and the semi-metal tellurium (Te). They can also occur without any direct contact with the major Cu-sulphide minerals as shown in Figure 30. There the complex composite grain consists mainly of isomertieite ($\text{Pd}_{11}\text{Sb}_2\text{As}_2$), sperrylite (PtAs_2) and chalcocite, and is found along the contact between calcite and plagioclase.

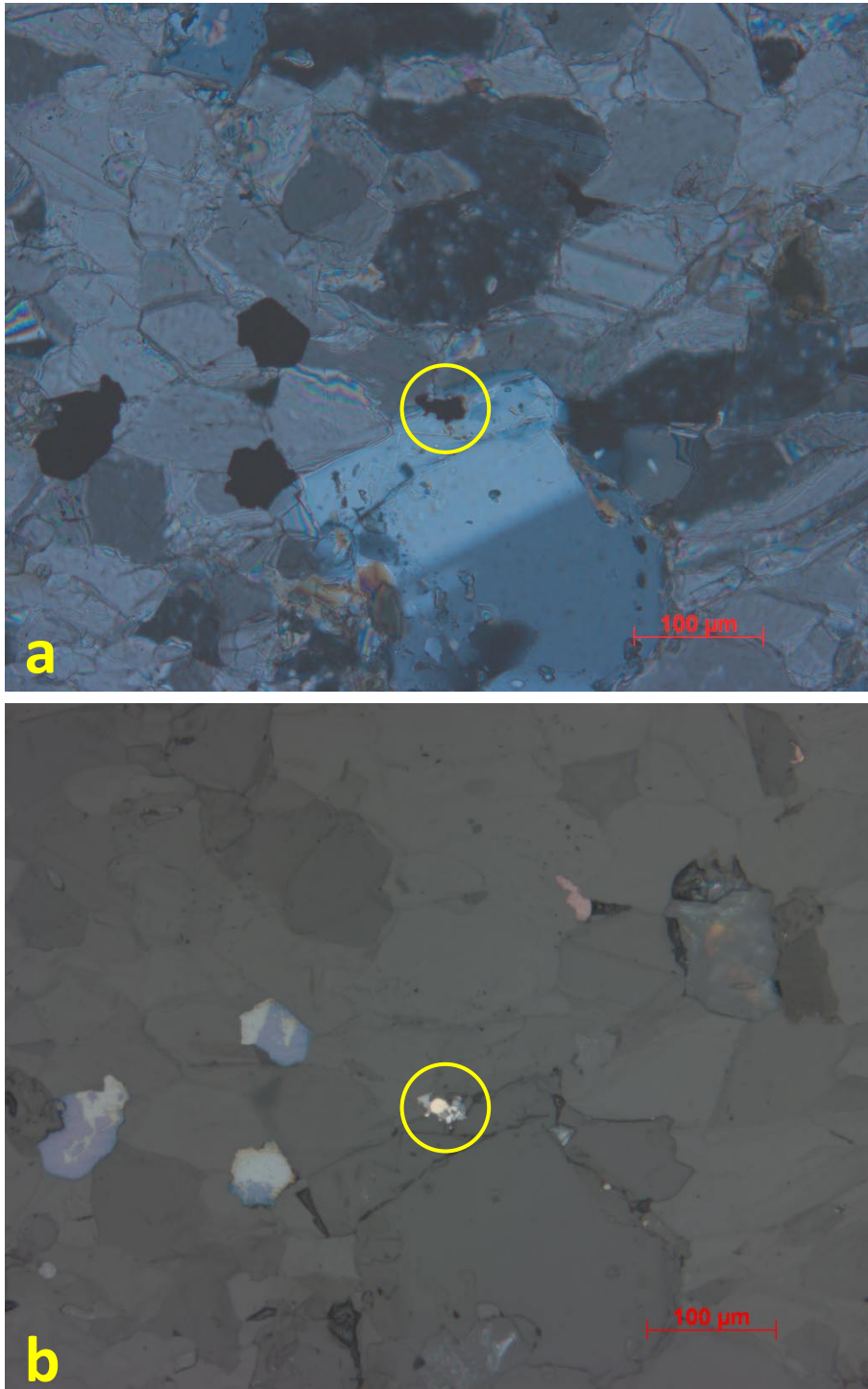


Figure 30: Photomicrographs of a composite grain of PGE-bearing minerals shown within the circles. a) At the grain boundary between plagioclase (white) and carbonate (brownish) (transmitted light). b) Clearly visible bright PGE-minerals and three composite grains of bornite (purple) and chalcocite (pale blue) in the middle left (reflected light)(sample H0814-17B).

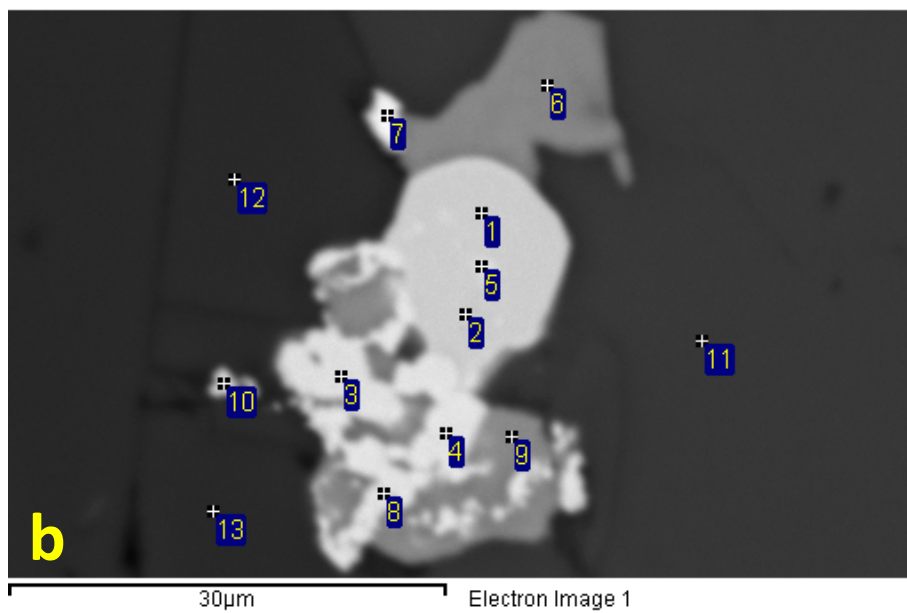
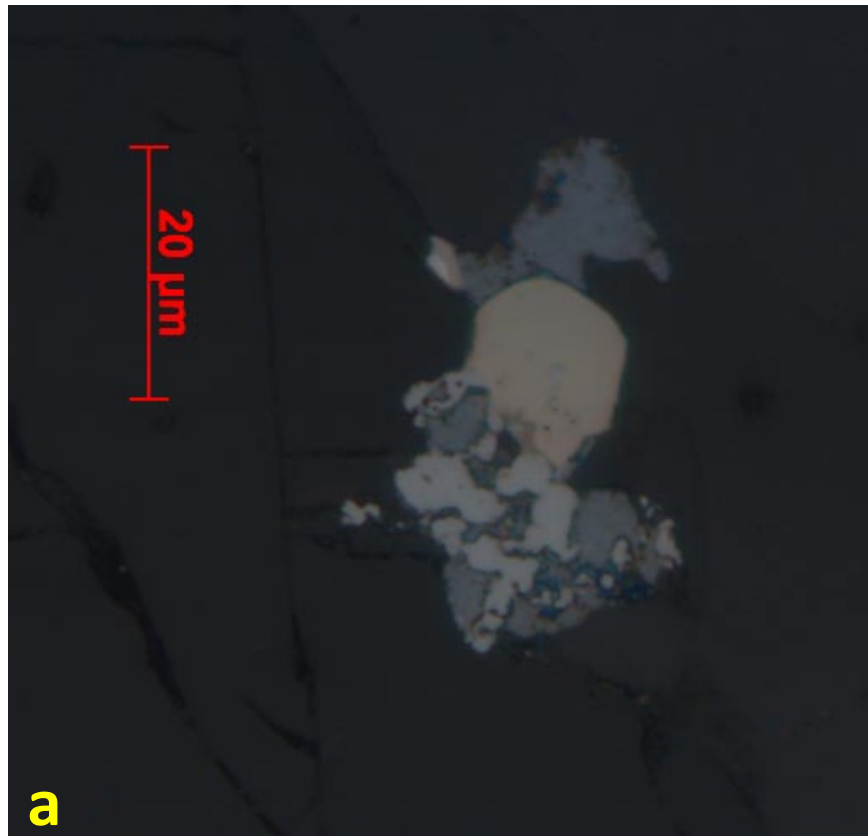


Figure 31a: Photomicrograph of the composite grain of PGE-bearing minerals in Figure 30 (reflected light). b: BSEM image of the same grain that consists of isomertieite (1,2,5? - $Pd_{11}Sb_2As_2$), sperrylite (3,4,8,10 - $PtAs_2$), unidentified PdAgBiHg mineral phase (7) and chalcocite (6,9) at the contact to calcite (11) and plagioclase (12,13) in sample H0814-17B. Numbers refer to analyses in Table 11.

Table 11: SEM analyses normalised to 100 weight% of minerals in Figure 31.

Anal.	Mineral	O	Na	Al	Si	S	Ca	Cu	As	Pd	Ag	Sb	Pt	Hg	Bi	Total
(all results in weight%)																
1	Isomertieite								9.69	73.98		16.34				100
2	Isomertieite								9.72	74.05		16.23				100
3	Sperrylite								36.62	3.12			60.26			100
4	Sperrylite								39.30				60.70			100
5	Isomertieite?								28.52	23.26		4.15	44.07			100
6	Chalcocite					23.14		76.86								100
7	PdAgBiHg?									32.80	5.05			58.08	4.07	100
8	Sperrylite								35.68	2.04			62.28			100
9	Chalcocite					24.14		75.86								100
10	Sperrylite								37.38				62.62			100
11	Calcite	58.34					41.66									100
12	Plagioclase	52.31	7.61	8.98	25.01		6.09									100
13	Plagioclase	51.87	7.76	9.13	25.71		5.53									100

In other part of the sample H0814-17B, the complex PGE-minerals are clearly associated with chalcocite and/or bornite. In Figure 32 inclusion of these are found both in wittichenite and chalcocite.

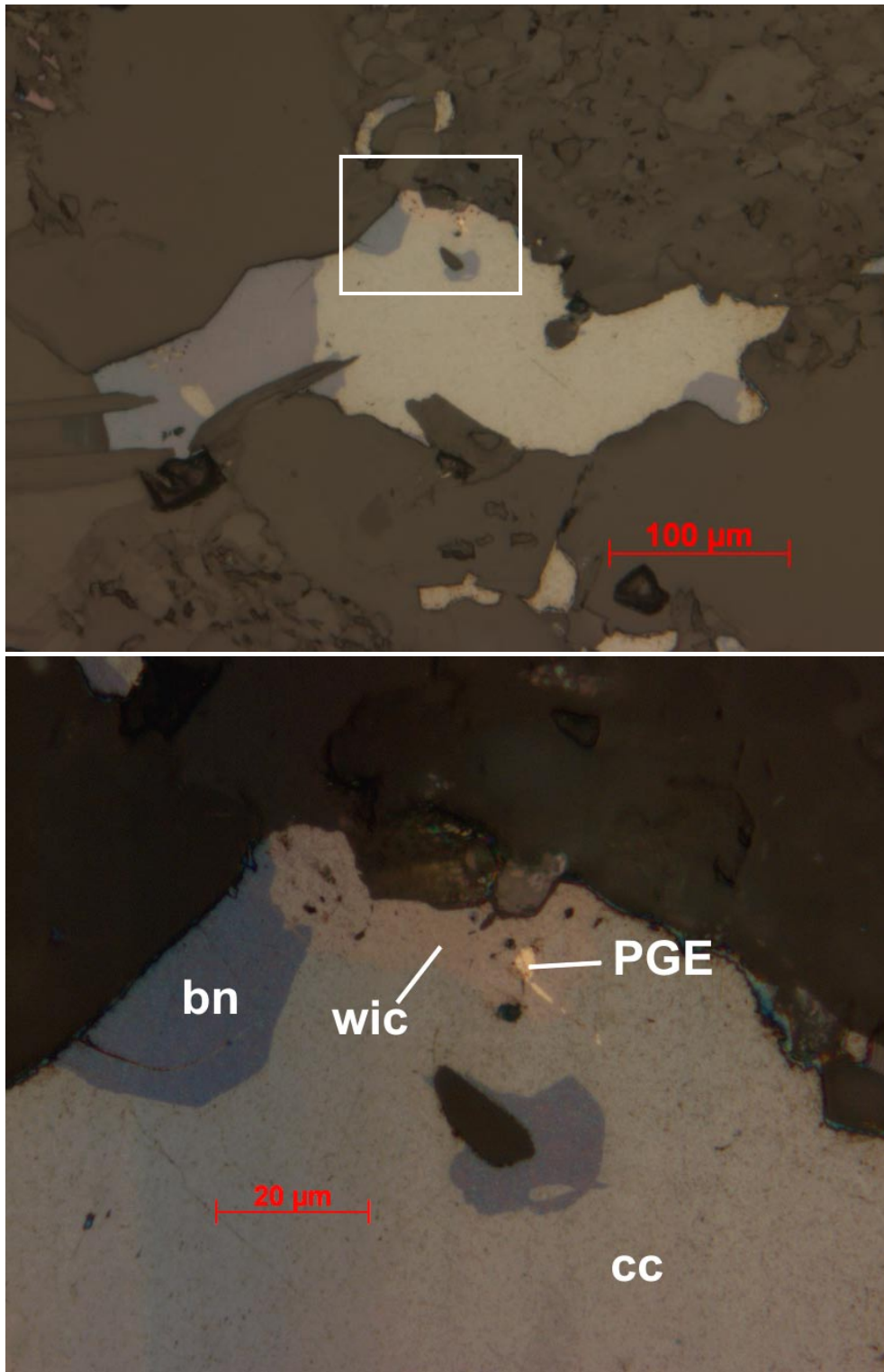


Figure 32: Photomicrographs of composite grains of chalcocite (cc - pale blue) and bornite (bn - purple) with wittichenite (wic - creamy) at the rim. The complex PGE-minerals (PGE - pale yellow) occur as inclusions in wittichenite and with a thin thread extending into chalcocite (see Figure 33) (sample H0814-17A – reflected light).

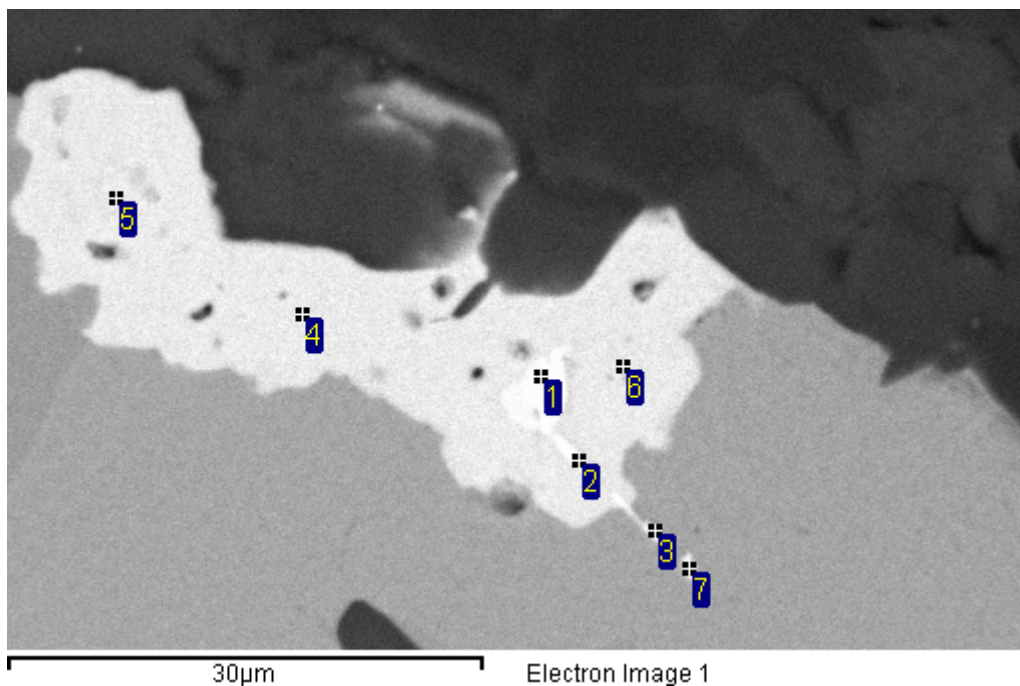


Figure 33: BSEM image of wittichenite (4,5,6) in Figure 32 with elongated aggregate of Pd-bearing telluride (1,2) that continues as a thin thread (7) into chalcocite and is associated with hessite (3). Numbers refers to analyses in Table 12.

Table 12: SEM analyses normalised to 100 weight% of minerals in Figure 33.

Anal.	Mineral	S	Cu	Pd	Ag	Te	Hg	Bi	Total
(all results in weight%)									
1	PdAgHgTe			32.99	9.50	42.91	14.61		100.00
2	PdHgTe			36.42		43.15	20.43		100.00
3	Hessite				57.28	42.72			100.00
4	Wittichenite	22.77	39.39					37.84	100.00
5	Wittichenite	24.51	38.66					36.83	100.00
6	Wittichenite	22.30	41.19					36.51	100.00
7	PdHgTe			35.74		43.80	20.46		100.00

5. MACROSCOPIC AND MICROSCOPIC DESCRIPTION OF SAMPLES

The macroscopic descriptions of each of the samples are accompanied by a photo of the cut cores and scanned images of the polished thin sections. For scaling; the size of the squares underlying the half cores are 10x10 mm and the size of the thin sections is 48x28 mm. The yellow frames in the photos of the cut cores show the location of the corresponding thin sections that are microscopically described below the figures. All the thin sections are oriented showing the right way-up in the lithological sequence.

H0810-01 117.5-117.8

The rock is composed of finely banded, fine-grained, greenish-grey sandstone and siltstone with minor carbonate-rich bands. Cu sulphides occur along lamina and veinlets that are concordant and sub-concordant to the sedimentary banding.



Figure 34: Photo of the cut core and scanned image of the thin section of sample H0810-01.

The sedimentary rock is finely banded on mm scale with alternating carbonate- and mica-rich bands with subangular to angular clastic grains of quartz and plagioclase. These bands are respectively whitish and greenish in Figure 34. The carbonate-rich bands contain around 1/3 of clastic grains. Elongated clastic grains and hypidiomorphic mica flakes are commonly oriented parallel to the sedimentary banding.

Bornite dominates among the Cu sulphides. Two varieties are seen in reflected light, both brown and purple. The purple variety commonly occurs together with chalcocite in composite grains. Myrmekitic intergrowth of bornite and chalcocite is also commonly observed. Chalcopyrite mainly occurs as minor (< 0.1 mm) scattered grains, but is also found intergrown with bornite.

Minerals	~vol %	Grain size	Comments
Quartz/plagioclase	30	~0.1-0.3 mm	Subangular to angular, both as individual and composite grains, coarse grained in irregular lenses/veinlets
Carbonate	10-60	≤ 0.1 mm	Xenomorphic grains comprise matrix to clastic grains

Biotite/muscovite	60-10	<<0.1-0.1 mm	Bt (pale brown) > mus
Bornite/chalcocite	5	~0.1-0.3 mm	Xenomorphic grains, bn (brown & purple) >cc
Chalcopyrite	Acc.	< 0.1 mm	

H0810-02 138.0-138.15

The sedimentary rock is irregularly banded with bands of greyish-green siltstone with irregular Cu-rich lenses and laminae that partly are discordant to the banding. Copper sulphides also occur in crosscutting veinlets.

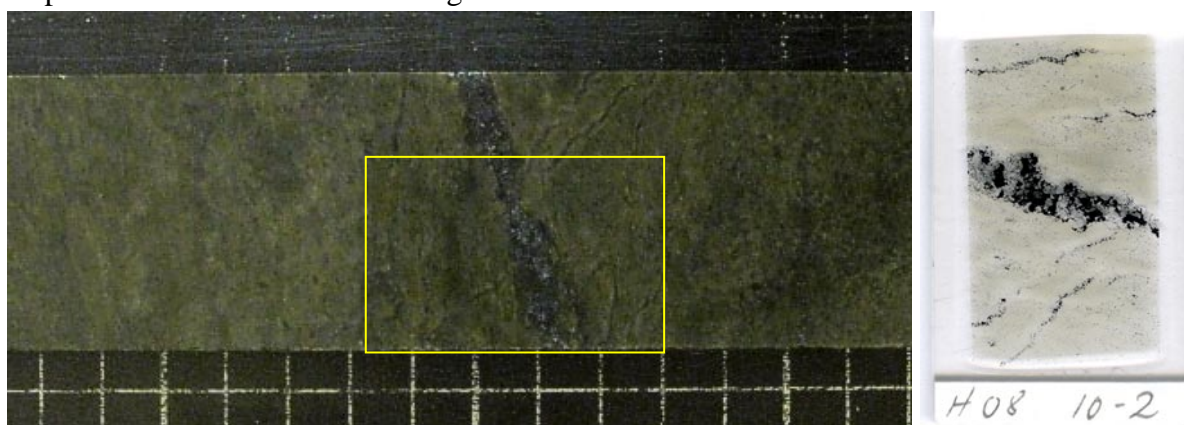


Figure 35: Photo of the cut core and scanned image of the thin section of sample H0810-02.

The rock is a fine-grained to very fine-grained and irregularly banded siltstone/mica schist that mainly contains muscovite (<< 0.1 mm) and minor quartz (\leq 0.05 mm). Biotite and needles of tourmaline also occur. In addition occur irregular lenses with subangular to angular quartz and feldspar grains (0.1-0.15 mm) and dominantly cross-cutting quartz-feldspar veinlets that are usually 0.2-1 mm thick. The tourmaline needles are oriented parallel to these veinlets.

Bornite is the dominant Cu sulphide and is enriched in bands and veinlets. In the 4-5 mm thick band/veinlet in the middle of the thin section (Figure 35) the grain sizes of bornite and chalcocite are 0.5-1.5 mm. More fine grained Cu sulphides occur in the thinner veinlets. A few grains of very fine grained chalcopyrite are found in the very fine grained muscovite-rich rock that overall contains just minor Cu sulphides.

H0810-03A/B 138.15-138.23

The sample is irregularly banded, and composed of partly sheared, greyish green, fine grained sandstone to siltstone with Cu sulphides enriched in bands (as H0810-02) and cross-cutting, irregular quartz-feldspar veins.

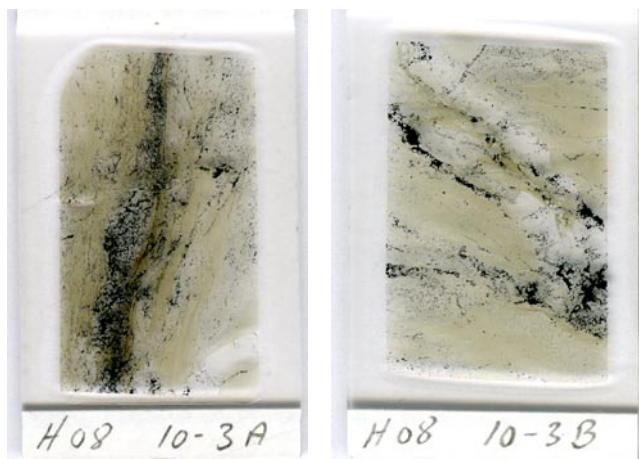


Figure 36: Scanned images of the thin sections of sample H0810-03.

This is a fine-grained and irregularly-banded siltstone similar to sample H0810-02 and is dominated by muscovite and quartz. In part of the sections very fine-grained muscovite dominates whereas in other parts fine-grained quartz (~0.1 mm) is the major mineral. Greenish (transmitted light) tourmaline is also found. Both the siltstone and the irregular quartz-feldspar veinlets are more strongly deformed than in H0810-02. The rock has experienced ductile shearing. The veinlets partly contain chlorite within, and along the contacts to the wall rock.

The Cu sulphides mainly occur in the irregular veinlets and along their contacts to the wall rock veinlets and as disseminations in the quartz-dominated siltstone. Bornite with variable grain sizes (0.2-1.5 mm) dominates. Some grains have an outer rim of chalcocite. Minor chalcopyrite is also found intergrown with bornite along its margin and internal cracks. Scattered grains of chalcopyrite are also enriched along crenulations cleavage.

H0810-06 135.8-136.0

The rock is composed of pale greyish-green, sheared and fine-grained sandstone to siltstone with thin lamina of Cu sulphides in the undeformed part. Cu sulphides are partly enriched along subconcordant quartz lenses/veinlets (to the right in Figure 37).

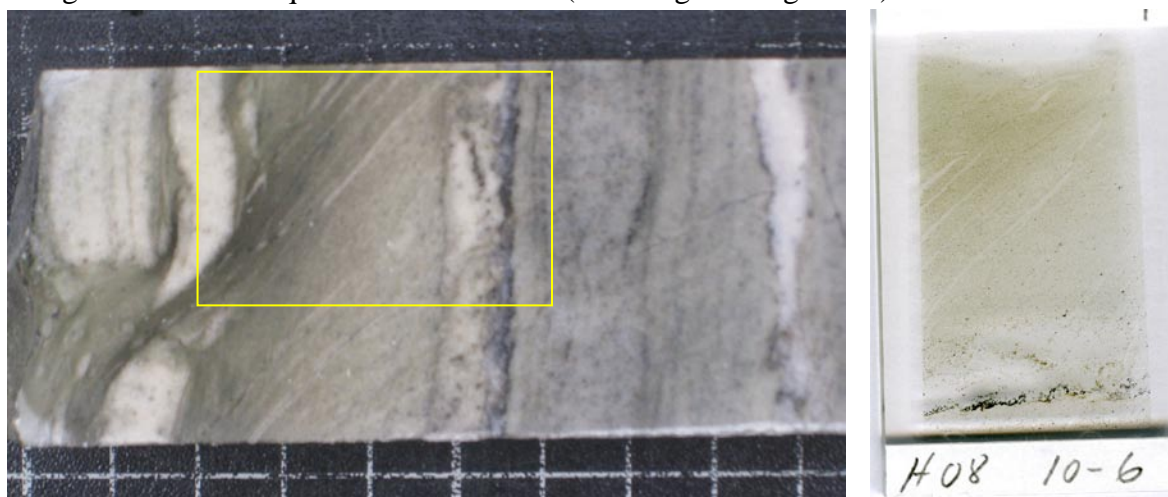


Figure 37: Photo of the cut core and scanned image of the thin section of sample H0810-06.

The thin section reveals a banded rock with whitish, fine grained quartz-feldspar-carbonate-rich bands in the upper and lower part of the thin section. The major, middle part consists of a fine- to very fine-grained fining-upward sequence with increasing content of mica towards the top. The upper part is clearly sheared and the extensional/C-plane/cleavage in the middle part comprise of fine-grained quartz veinlets without Cu sulphides. This cleavage ends above the Cu sulphide rich band at the bottom.

Minerals	~vol %	Grain size	Comments
<i>Middle part:</i>			
Quartz/plagioclase	20-40	~0.05-0.15 mm	Subangular to angular, more angular upwards, partly orientated along C-plane
Carbonate	30-50	<<0.1 mm	Xenomorphic grains comprise matrix to qtz/pl, decreasing content upwards
Biotite/muscovite	10-30	<<0.1 mm	Bt (brownish) ~ mus, increasing content upwards
Bornite/chalcopyrite	≤1	<<0.1 mm	
<i>Upper/lower part:</i>			
Quartz/plagioclase	60/40	0.1-0.2 mm	Xenomorphic grains
Carbonate		0.1-0.2 mm	Xenomorphic grains
Biotite/muscovite	0-5		Bt (dark brown) ~ mus
Bornite/chalcocite	0/5	0.1-0.2 mm	Xenomorphic grains/aggregates, bn (brown & purple) >cc

H0810-09 136.24-136.36

The sample comprises greyish white, fine-grained sandstone to siltstone with some carbonate-rich bands and shows irregular, lens-formed fabric. Strong dissemination of Cu sulphides occurs in irregular bands and lamina. It contains quartz-rich bands that could represent recrystallised chert.



Figure 38: Scanned image of the thin section of sample H0810-09.

In thin section the rock shows a very irregularly banded texture with highly variable grain sizes; << 0.01-2.5 mm. The lower part comprises alternating bands dominated by fine-grained (≤ 0.05 mm) quartz (95 vol%) and carbonate and more fine- to medium-grained irregular lenses/bands of quartz and carbonate in various proportions. The upper part has a more variable composition and grain size with higher contents of biotite and chlorite (Mg-rich chlorite that is colourless in transmitted light).

The Cu-sulphides are enriched in irregular aggregates, mostly in the upper part of the section with similar proportions of bornite and chalcocite (0.1-1 mm). Both purple and brown bornite exists and myrmekitic intergrowth of bornite and chalcocite is common.

H0810-10 136.36-136.48

This sample is pale greyish sandstone grading upwards into reddish siltstone capped by irregular carbonate-sandstone band. The banded rock is cross-cut by irregular quartz veinlets. Cu sulphides occur as disseminations in sandstone and in quartz veinlets, and are partly enriched in the irregular sandstone bands on top of the siltstone.

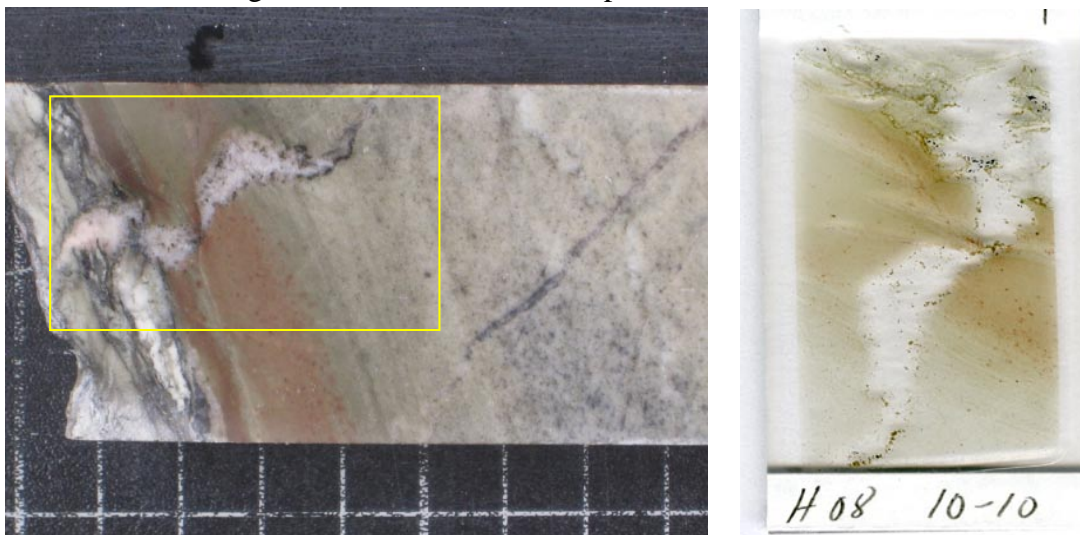


Figure 39: Photo of the cut core and scanned image of the thin section of sample H0810-10.

The sandstone in the lower part of the thin section consists of around 40 vol% of clastic grains of quartz and plagioclase in a matrix of xenomorphic carbonate and a few grains of biotite. The amount of biotite increases and the contents of clastic grains and carbonate decrease in a fining-upwards sequence in the reddish-coloured part of the sample. A few, very fine-grained xenomorphic grains of bornite and chalcocite occur. More irregular banded and partly sheared carbonate-bearing sandstone with minor Cu sulphides are found at the top of the thin section.

The cross-cutting vein is 2-6 mm thick and partly zoned. The core comprises carbonate and is enveloped by quartz that has grown perpendicular to the walls of the vein - open-space filling. Biotite occurs along the rim of the vein. The vein is affected by ductile shearing and minor brittle faulting that indicates complex or several phases of deformation. A few aggregates of bornite (brown and purple) and chalcocite are found in the vein.

H0811-11 139.2-139.5

The siltstone in the sample is finely banded greyish green and pale yellow, and is strongly folded and shear-deformed. Strong dissemination of Cu sulphides occurs in quartz-rich folded bands and veinlets along the axial cleavage.

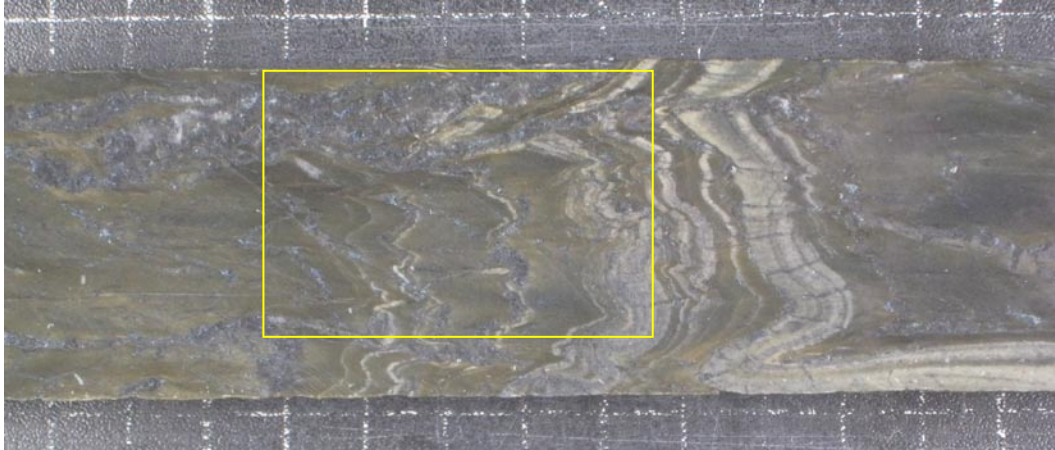


Figure 40: Photo of the cut core and scanned image of the thin section of sample H0811-11.

The fine-grained bands comprise around 70-80 vol% of clastic grains of quartz and feldspar (≤ 0.1 mm) and minor mica ($\ll 0.1$ mm - 5-10 vol%) and sulphide minerals (5-10 vol%). The very fine grained bands are dominated by muscovite and minor biotite ($\ll 0.1$ mm - 95 vol%) and 1-2 vol% of Cu-sulphide minerals. Tourmaline occurs as accessory mineral. The axial plane cleavage of minor folds is clearly expressed by alignment of Cu sulphides (dominantly chalcopyrite) and mica minerals. In addition there are strongly deformed veinlets and lenses of fine- to medium-grained (0.2-0.8 mm), recrystallised quartz. They are partly oriented along the cleavage.

The Cu-sulphide minerals comprise about equal amounts of bornite and chalcocite. Their grain sizes vary according to the host rock. Aggregates of these are also enriched within the quartz veinlets/lenses. The formation of most of the Cu sulphides is assumed to pre-date the folding and shearing, but chalcopyrite seems to have been deposited syntectonically along the axial plane cleavage.

H0811-13 142.5-142.65

The sample is composed of greenish-grey sandstone overlain by grayish-green siltstone. Dissemination of Cu sulphides increases up towards the siltstone. There are cross-cutting fractures filled with Cu sulphides in the siltstone.

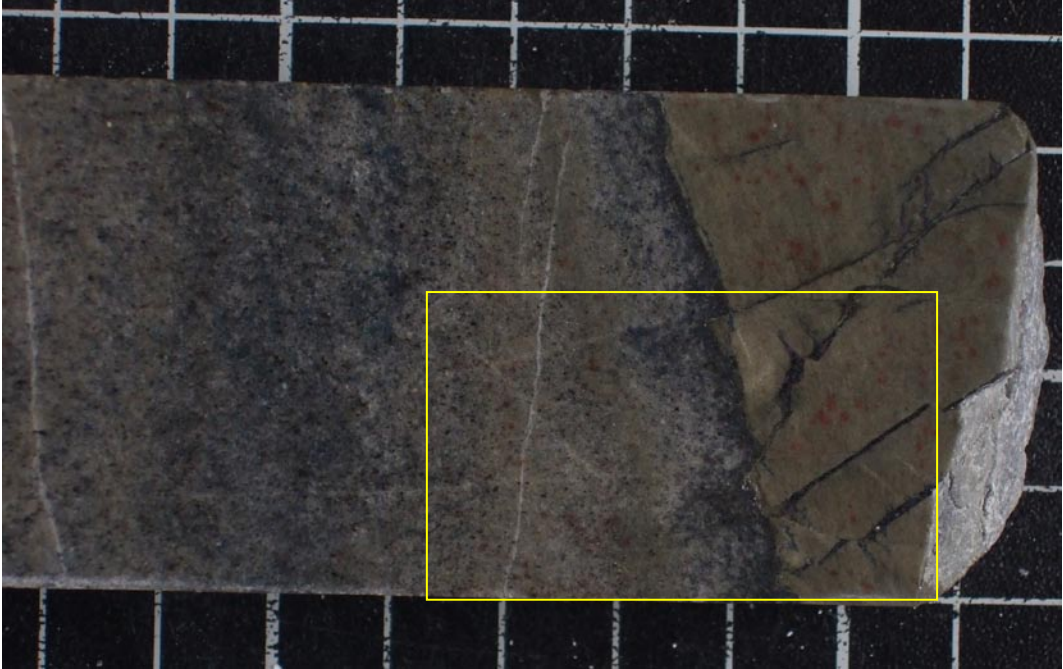


Figure 41: Photo of the cut core and scanned image of the thin section of sample H0811-13. The most carbonate-rich middle layer is marked with yellow dotted lines. Note the cracks in the upper siltstone layer. They are mainly filled with bornite, biotite and quartz.

The lower half of the thin section consists of fine-grained, diffusely layered carbonate-bearing sandstone that is overlain by very fine-grained siltstone. The siltstone and upper part of the sandstone have experienced brittle fracturing with various orientation and with associated Cu sulphide formation.

The sandstone consists of three diffuse bands that comprise:

Minerals	~vol %	Grain size	Comments
<i>Lower layer:</i>			
Quartz/plagioclase	~30	~0.1 mm	Angular to subangular grains
Carbonate	50-60		Xenomorphic, matrix
Biotite	5		Brownish aggregates
Bornite/chalcopyrite	5	<0.05-0.1 mm	Xenomorphic grains, bn (brown & purple) >cc
<i>Middle layer:</i>			
<i>Greenish grey coloured in thin section (Figure 41)</i>			
Quartz/plagioclase	10-15	0.05 mm	
Carbonate	70-75		
Biotite	10		Dark brown
Bornite/chalcocite	1-2		
<i>Upper layer:</i>			
Quartz/plagioclase	50-60		
Carbonate	5		
Biotite	5-10		Increasing content up towards siltstone
Bornite/chalcocite	10-30		Xenomorphic grains, increasing content up towards siltstone

The lowest content of Cu sulphides is found in the carbonate-rich middle layer, whereas this content increases substantially near the border to overlying siltstone. Bornite (purple and brown) and chalcocite most commonly comprise interstitial grain between the clastic grains of quartz and feldspar. The grain sizes of the sulphides correspond with the grain sizes of the host rock.

The siltstone comprises very fine-grained (< 0.05 mm) quartz, feldspar and mica. Biotite and muscovite as well as minor amounts of tourmaline also occur. Biotite commonly comprises aggregates in association with the opaque minerals. Common accessory minerals include rutile and unidentified U- and Th-bearing minerals.

The siltstone is crosscut by 1-2 mm thick Cu sulphide-biotite-quartz veinlets that are deposited along fractures. These veinlets are themselves crosscut by minor fractures. Electrum (AgAu) is found as tiny inclusions (3-4 µm) in bornite in the siltstone and in association with chalcocite along a crack in bornite in a cross-cutting veinlet.

H0811-14 143.5-143.75

The sample is composed of strongly sheared, dark greenish fine-grained sandstone and siltstone with gradual yellowish bleaching. Cu sulphides are enriched along lamina concordant to the shearing as well as along cross-cutting veinlets. Note that this sample was collected only 1 m from sample H0811-13 that shows very little ductile deformation.

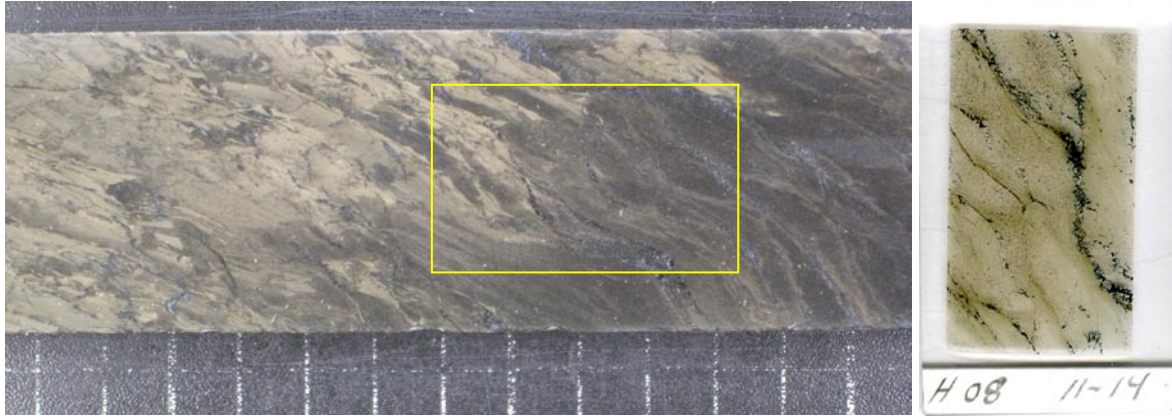


Figure 42: Photo of the cut core and scanned image of the thin section of sample H0811-14.

The composition of the rock is similar to that of sample H0811-11, which also shows strong ductile shearing. It comprises bands and lenses dominated by fine-grained, angular to sub-angular quartz and feldspar (≤ 0.1 mm - 70-80 vol%), minor mica ($\ll 0.1$ mm - 5-10 vol% - mainly biotite) and Cu sulphide minerals (5-10 vol%) alternating with bands and lenses of very fine-grained mica, mainly muscovite ($\ll 0.1$ mm - 80-90 vol%), quartz/feldspar and tourmaline. Both plagioclase and K-feldspar are found. The colour change in the core is due to lenses/bands dominated by muscovite (yellowish) and more biotite-bearing, quartz-feldspar-rich greenish bands/lenses. This colour change may indicate alteration phenomena, but studies so far suggest a primary sedimentary transition modified by later ductile deformation.

The Cu-sulphide minerals comprise bornite and chalcopyrite that are disseminated in sandstone bands and lenses as well as being enriched along shear structures. Minor Cu sulphides occur in the very fine-grained siltstone lenses/bands, most frequently bornite but with minor chalcopyrite and chalcocite. Replacement of bornite by covellite is found in a few grains.

H0811-15 144.0-144.1

The sandstone of the sample is dark greenish, fine-grained and irregularly deformed. It contains strong Cu-mineralisations, partly as veinlets/cracks.

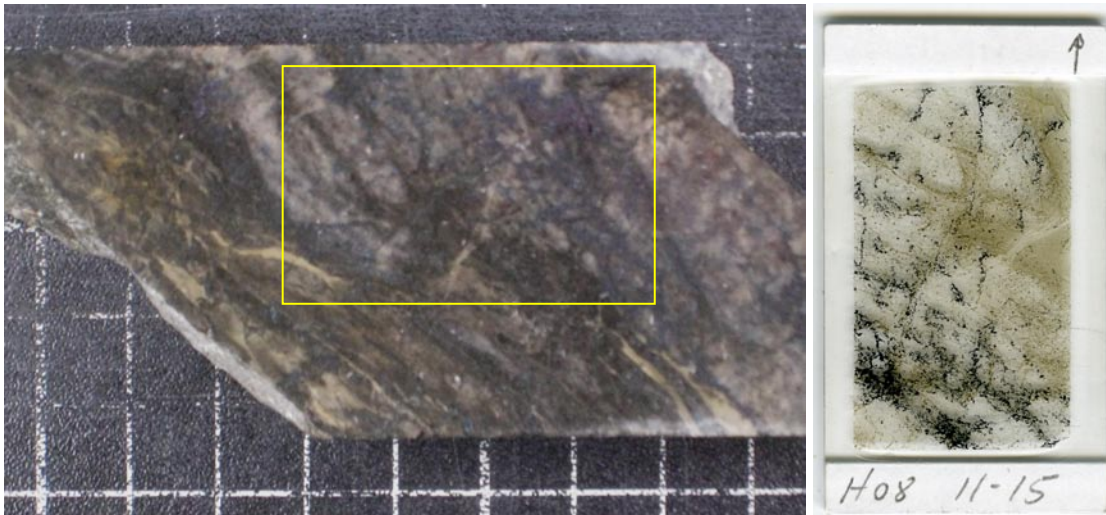


Figure 43: Photo of the cut core and scanned image of the thin section of sample H0811-15.

Most of the thin section comprises fine-grained (0.1-0.3 mm) quartz, plagioclase and K-feldspar with some interstitial fine-grained biotite and minor muscovite. The rock is weakly foliated and cross-cut by thin quartz veinlets. The right part of the section is dominated by very fine-grained ($\ll 0.1$ mm) aggregates of mica containing few clastic grains of quartz and feldspar. Accessory minerals in the sandstone include barite and rutile as well as unidentified Th and U mineral phases.

The Cu sulphides, mainly bornite and chalcocite are enriched along medium-grained, irregular quartz veinlets and as aggregates in the sandstone. Bornite, both purple and brown is more common than chalcocite. Minor replacements of bornite by chalcopyrite occur along cracks and grain boundaries. Very fine-grained chalcopyrite is also disseminated in the sandstone. Several tiny grains of sperrylite (PtAs_2) occur, and hessite (AgTe) is accessory mineral.

H0811-16 144.1-144.2

The sample comprises pale grey sandstone which shows gradual transition to dark grey sandstone with yellowish siltstone clasts/fragments. Locally strong dissemination of Cu sulphides occurs.

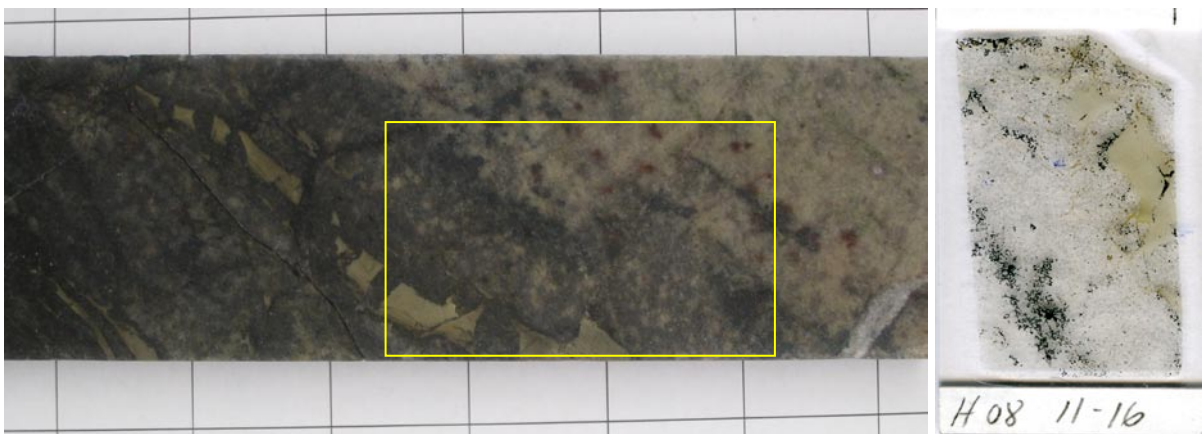


Figure 44: Photo of the cut core and scanned image of the thin section of sample H0811-16.

The major part of the thin section comprises sandstone with fine-grained (0.1-0.2 mm), sub-angular to sub-rounded clasts of quartz and feldspar, both plagioclase and K-feldspar. Carbonate and mica comprise, in total 5-10 vol% of the pale-coloured sandstone and their contents increase upwards into the darker grey part of the rock. Accessory minerals include barite and rutile. The yellowish angular clasts/fragments or broken bands of siltstone, dominantly consist of very fine-grained mica and minor amounts of quartz, feldspar and tourmaline.

The Cu sulphides are both enriched as interstitial grains forming bands/layers in the sandstone (commonly 0.1-0.2 mm, up to 1 mm) and along veinlets in and between the siltstone clasts. Bornite dominates over chalcocite, and a few tiny grains of chalcopyrite are disseminated interstitially in the sandstone and fill cracks in bornite.

H0814-17A/B 320.45-320.7

The sample is composed of greyish-white, banded carbonate-rich sandstone that is locally folded and sheared. Cu sulphides are enriched in thin lamina.

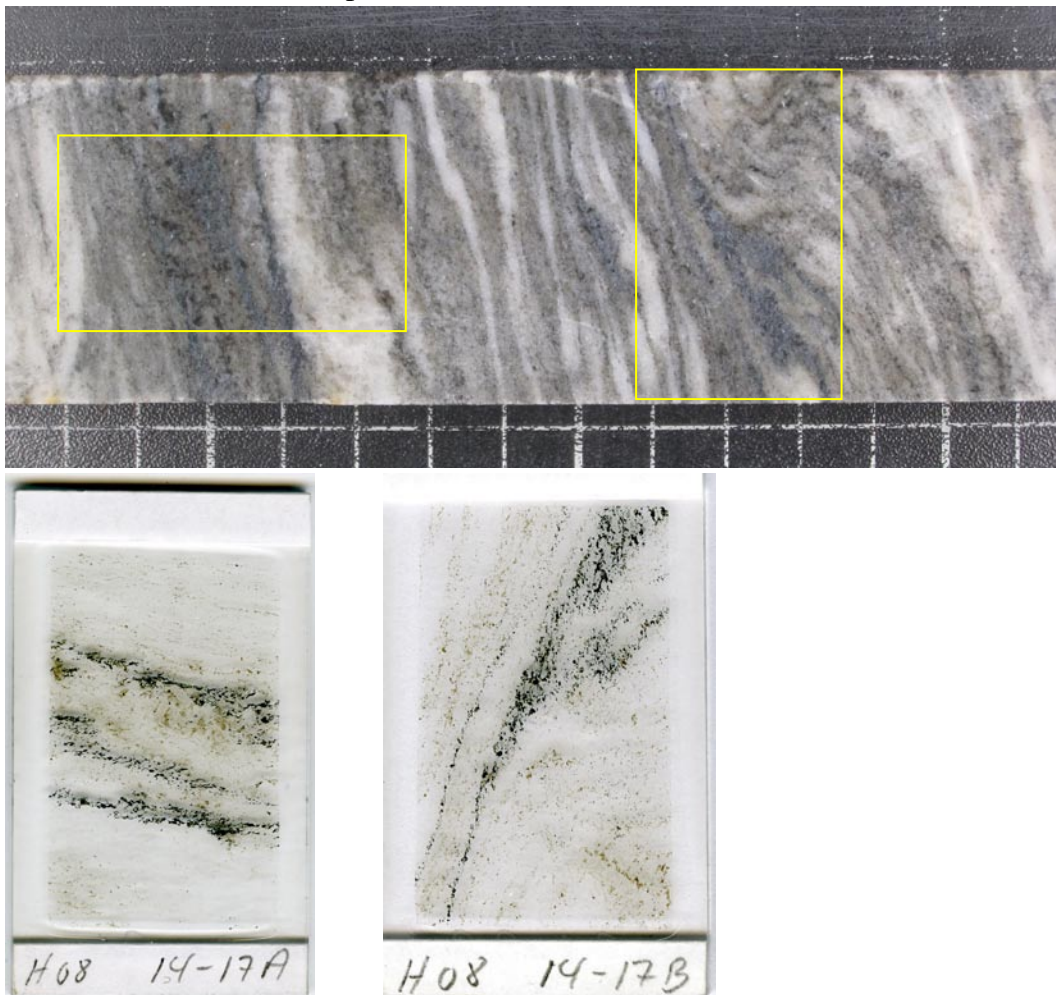


Figure 45: Photo of the cut core and scanned images of the thin sections of sample H0814-17.

The upper and lower parts of the thin section -17A are dominated by xenomorphic, recrystallised, fine-grained carbonate (0.05-0.1 mm - 85-95 vol%) and minor quartz, feldspar and biotite (5-15 vol%). Calcite is the major carbonate mineral. The Cu sulphides are enriched in conjunction with aggregates of chlorite and biotite in diffuse layers that contain more

quartz, chlorite and biotite in the middle part of the section. A similar carbonate-rich rock occurs in thin section 17B. In this sample the orientation of the Cu sulphide-rich layers are sub-concordant to the foliation. Accessory minerals include barite and monazite (5-25 μm).

Bornite and chalcocite are the most common Cu-sulphide minerals and comprise interstitial grains (0.1-1.0 mm). Elongated grains are commonly oriented along the foliation. As in the others samples both purple and brown bornite occur. Composite grains of both bornite and chalcocite as well as myrmekitic intergrowth of these are also common. Only a few, tiny grains of chalcopyrite occur, mostly as replacement of bornite. Wittichenite (Cu_3BiS_3) is a common accessory mineral associated dominantly with bornite. The amount and variety of noble metal-bearing minerals are greater in these sections and include amalgam (AgHg), hessite (AgTe), sperrylite (PtAs_2), bohdanowiczite (AgBiSe_2) and unidentified AgPbSe mineral phase, often associated with clausthalite (PbSe) and native bismuth (Bi). Pd is also found in unidentified PdHgTe and PdBiHg mineral phases which can be Ag-bearing.

H0814-19 321.2-321.32

The sample is composed of pale greenish-grey, banded sandstone and siltstone with carbonate-rich sandstone and reddish siltstone/chert. Cu sulphides are enriched in concordant lamina.

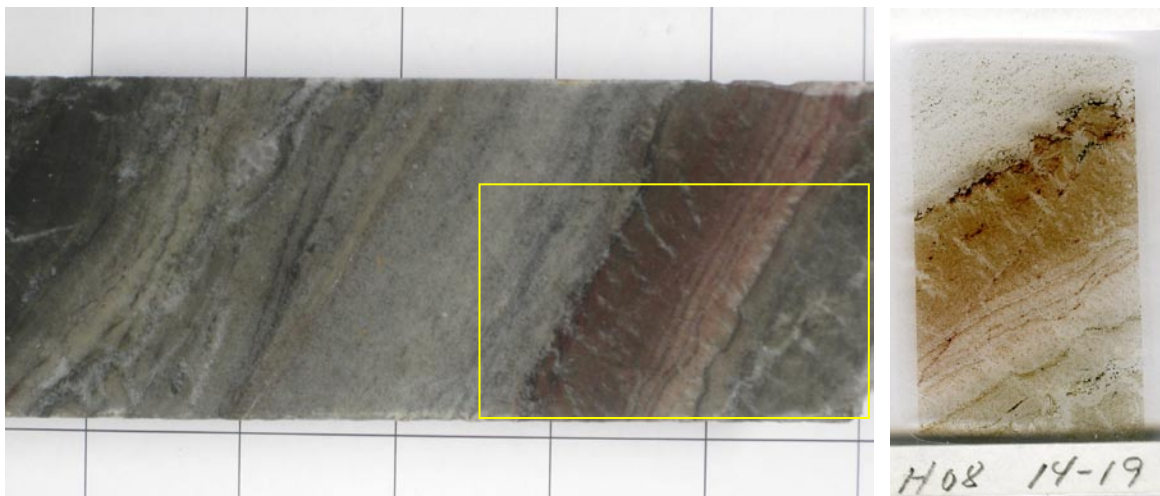


Figure 46: Photo of the cut core and scanned image of the thin section of sample H0814-19.

The brownish (reddish in photo of core), middle part of the thin section comprises very fine-grained siltstone with 50-60 vol% biotite and minor quartz/feldspar and carbonate. This layer is crosscut by minor, parallel carbonate veinlets that may have formed along a secondary cleavage. Cu sulphides are enriched in thin bands in the upper part of the layer. On top of the siltstone occurs a carbonate-rich layer (pale grey coloured) that comprises around 90 vol% carbonate with minor quartz and biotite.

The Cu sulphides comprise mainly bornite and chalcocite. As opposed to the other samples, brown-coloured bornite shows myrmekitic intergrowth with chalcocite (or digenite?). A few grains of chalcopyrite and covellite also occur.

H0821-20 127.4-127.6

The sandstone is fine-grained, banded and pale greyish green in the core sample. Cu sulphides are enriched in layers and lamina.

Figure 47: Scanned image of the thin section of sample H0821-20.



The rock is layered rock with alternating fine-grained sandstone and very fine-grained siltstone layers. The Cu sulphides are mostly enriched in the sandstone layers that comprise xenomorphic, sub-angular to sub-rounded clastic grains of quartz and feldspar (0.05-0.15 mm) with minor mica and tourmaline. Some minor aggregates of carbonates occur in the sandstone. The siltstone layers are dominated by very fine-grained mica. As opposed to most of the other examined samples, muscovite is the dominant mica. Whether this is related to alteration/sericitisation or is a primary feature is not clarified so far. Accessory minerals include rutile, barite, monazite and zircon.

This is probably the most copper-rich sample studied, and the Cu sulphides mainly comprise interstitial grains with grain size variations in accordance to the grain sizes of the clastic grains. Bornite (brown and purple) and chalcocite are the dominant Cu sulphides. Myrmekitic intergrowth and composite grains of these minerals are also common. Only a few tiny chalcopyrite grains occur.

6. DISCUSSION

The main aims of the study were to describe the various Cu-sulphide minerals and to identify the noble metal-bearing minerals and their relationship to the Cu sulphides. The occurrence of the major Cu-sulphide minerals bornite and chalcocite are well documented using optical microscopy and by scanning electron microscope (SEM). Several accessory sulphide minerals including chalcopyrite, covellite, wittichenite, carrolite and cinnabar are also clearly verified, except for wittichenite which might represent another unnamed Cu-Bi sulphosalt.

The identification of the noble metal-bearing minerals is not as straightforward and warrants comments as the results may have implications for the possible exploitation of these metals.

In a gold deposit, gold is typically distributed in (Cook 2001):

- Native gold, electrum and amalgam (alloys of Au,Ag,Hg) (i.e. gold visible for the naked eye or by optical microscopy).
- Other Au-bearing minerals, especially Au- and Ag-Au-tellurides (e.g. cavalierite AuTe_2 which is an important constituent in some of the gold ore in the Bidjovagge Au-Cu deposit (Ekberg & Sotka 1992)).
- 'Invisible gold', that is gold within the common sulphides and oxides, either as sub-microscopic ($< 1 \mu\text{m}$) grains or bound in the crystal lattice (refractory gold) (Cabri 1992).

In the studied samples only five grains of microscopic visible gold have been identified. Both electrum and amalgam occur with grain sizes in the range 3-15 μm , while no other Au-bearing minerals have been found. Thus, the amount of Au minerals found so far may not explain the gold contents in the analysed cores (Appendix 1). Substantial amounts of 'invisible gold' may exist in the Nussir deposit, but further SEM studies are required to clarify this. Both bornite and haematite in the sediment-hosted copper deposits in the Kupferschiefer in Poland contain significant amounts of gold, ranging from 0.21 to 1.27 wt% in bornite (Piestrzyński et al. 2002). 'Invisible gold' is possible as long as the Nussir mineralisations have not experienced amphibolite-grade metamorphism. Gold is more likely to be released from the lattice in ore deposits regionally metamorphosed at amphibolite grade or above.

Similar considerations could also be made for silver as lattice-bound silver is common in sulphides (Cabri 1992) although Ag-bearing minerals are more abundant in some of the studied samples. These minerals are clearly associated with the major Cu sulphides and should be relatively easily processed. The major silver minerals in the Rudna ore body in Kupferschiefer in Polen are stromeyerite (AgCuS), native silver, amalgams, electrum, acanthite (Ag_2S) and jalpaite (Ag_3CuS_2), but the major Cu sulphides are also Ag-bearing (Suchan 2001).

The sampling of the PGE-rich intervals in the cores H0811 and H0814 seems to have been quite successful, both the samples H0811-15 and H0814-17A/B contain significant amounts of PGE-minerals. Most Pt-minerals were identified in the fine-grained sandstone sample

(H0811-15) as sperrylite (PtAs_2), but their relationship to the major Cu sulphides is unequivocal. The PGE mineralogy is more complex in the carbonate-sandstone in samples H08-17A/B, and the PGMs also occur both within and without any intergrowth with bornite and chalcocite. An association between Pd and Ag is shown by the unidentified Ag-bearing PdHgTe and PdBiHg mineral phases.

The formation of major sediment-hosted copper deposits globally has been broadly studied and discussed in the literature and their origin has been classified into three principal groups: syngenetic, diagenetic and epigenetic (Brown 1993). Today, there seems to be a general agreement that the sulphides postdate the sedimentation, but available evidence suggests that the deposits can form at several stages during the evolution of the sedimentary basin from early diagenesis of host sediments through basin deformation and metamorphism. A prerequisite for formation of supergiant (> 24 Mt contained Cu) and giant ore deposits seems to be a long period of hydrothermal fluid flow and mineralisation in a closed basin (Hitzman et al. 2005). Only three basins contain supergiant deposits; the Palaeoproterozoic Kadora-Udokan basin in Russia, the Neoproterozoic Katangan basin (Central African Copperbelt) in Zambia and the DR Congo and the Permian Zechstein basin (Kupferschiefer in Poland and Germany) (Hitzman et al. 2005). Most studies favour an early to late diagenetic formation of the copper mineralisations with associated gold, platinum and palladium mineralisations in the Kupferschiefer in Poland (Oszczepalski 1999, Piestrzyński et al. 2002).

The present study is too limited to give any conclusive statements regarding the formation and timing of the copper and noble-metals mineralisations in the Nussir deposit, but some indications of the relative timing of the formation of various minerals are suggested. The major Cu sulphides, bornite and chalcocite commonly comprise interstitial grains and aggregates in the sandstone matrix. They thus fill the interstices between the clastic silicate grains which may indicate diagenetic formation of the major copper mineralisation, although later re-mobilisation is recorded.

The texture in sample H0811-13 gives indications of late-diagenetic upward migrations of copper-bearing fluids. Cu sulphides are clearly enriched in the uppermost part of the sandstone layer (Figure 41). The fractures in the siltstone can be interpreted either as the result of syn-sedimentary faulting with further migration of the fluids in partly lithified sediments or late brittle fracturing with re-mobilisation of bornite.

Bornite and chalcocite may be contemporaneous, although bornite seems to be replaced by chalcocite to some extent. Chalcopyrite partly replaces bornite (Figure 8). The formation of chalcopyrite seems also to be related to late ductile deformation as shown in sample H0811-11 (Figure 9). The major Cu sulphides may also be replaced by wittichenite (Figure 10), although the partly graphic exsolution of wittichenite and associated Ag-bearing minerals can also have been formed during regional metamorphism. Alternatively they have been formed through epitactic growth. The complex mineralogy also suggests that a prolonged period of fluid flows with several pulses is likely in the basin.

The timing of formation of the noble metal-bearing minerals is hard to define. Electrum is found as inclusions (exsolution caused by metamorphism?) in bornite in sample H0811-13 (Figure 14), but is also clearly mobilised along cracks in bornite in the same sample (Figure 17). Sperrylite is found as inclusions surrounded by cobaltite in composite bornite-chalcocite grains (Figure 27), but also envelopes chalcocite (Figure 29). The other grains of sperrylite are more randomly distributed. The formation of the more complex PGE mineralogy observed in the carbonate-rich samples H0814-17A/B seems to be more closely associated silver-bismuth-tellurium mineralisation. The question of whether this is lithologically controlled or not needs further studies.

Unusually, for many sulphide deposit, not a single Fe-sulphide mineral was detected in the studied thin sections, although it is known that pyrite exists in other part of the deposit. Low sulphur concentration in the hydrothermal fluids is also indicated by the preference for formation of Cu-rich sulphide minerals. The low iron content of the system is also demonstrated by the fact that the major Ti-bearing mineral is rutile, and additionally minor titanite is identified, but ilmenite is not observed.

It is obvious that further studies are required to evaluate the suggestion proposed and to get a better understanding of the formation and evolution of the Nussir copper deposit that is enriched in silver, gold, platinum and palladium.

7. CONCLUSION

The host rocks of the Nussir copper deposit are fine-grained sandstones and siltstones that contain carbonate-rich layers. They are heterogeneously deformed and both rocks with well-preserved primary layering and rocks that exhibit strong ductile deformation have been studied.

The major copper sulphides, bornite and chalcocite mainly comprise cement for the clastic grains of the sandstone, which may suggest a syngenetic or diagenetic origin for their deposition rather than strictly epigenetic formation related to deformation of the host rock. Accessory sulphide minerals include chalcopyrite, covellite, wittichenite, carrolite and cinnabar. They appear to occur as replacement for and/or exsolution from the major Cu sulphides. Alternatively they may also have been formed through epitactic growth. They are partly formed during later deformation and regional metamorphism.

Gold and silver are closely associated with the Cu mineralisations. Electrum (3-15 μm) is found in contact with, as inclusions in and in cracks in bornite. Additionally, silver occurs in hessite, Ag-bearing clausthalite, bohdanowiczite, naumannite and unidentified AgBiTe mineral phase, often associated native bismuth and wittichenite. These minerals commonly comprise exsolutions or droplets in the major Cu sulphides and are often enriched at their rims.

Platinum most frequently occurs as microscopic grains of sperrylite that form clusters of inclusions in bornite and disseminated, interstitial grains in the silicate matrix of the sandstone. Palladium is a minor constituent of some sperrylite, but more commonly comprises complex grains of isomertietite and unidentified PdHgTe and PdBiHg mineral phases which can be Ag-bearing, both in contact with, and separate from the major Cu sulphides. A very complex metal mineralogy is observed in the carbonate-rich rock sample, but the question of whether this is lithologically controlled or not needs further studies.

8. REFERENCES

- Brown, A.C. 1993: Sediment-hosted stratiform copper deposits. Geological Association of Canada Reprint Series 6, v. 2, p. 99-116.
- Cook, N.J. 2001: Ore mineralogical investigation of the Mofjell deposit with emphasis on gold and silver distribution. NGU Report 2001.051, 31 p.
- Ekberg, M. & Sotka, P. 1991: Production mineralogy and selective mining at Bidjovagge mine, northern Norway. International Conference on Applied Mineralogy, Pretoria, South Africa.
- Hitzman, M., Kirkham, R., Broughton, D., Thorson, J. & Selley, D. 2005: The Sediment-hosted Stratiform Copper Ore System. SEG 100th Anniversary Volume, p. 609-642.
- Oszczepalski, S. 1999: Origin of the Kupferschiefer polymetallic mineralization in Poland. Mineralium Deposita 34, p. 599-613.
- Piestrzyński, A., Pieczonka, J. & Gluszek, A. 2002: Redbed-type gold mineralisation, Kupferschiefer, south-west Poland. Mineralium Deposita 37, p. 512-528.
- Suchan, J. 2001: Silver distribution in the Rudna mine district, Poland. Piestrzyński, A. et al (eds.): Mineral Deposits at the Beginning of the 21st century. Balkema Publ., p. 247-251.

Appendix 1: Chemical analyses of core samples from the Nussir copper deposit. All results in ppm if otherwise are not stated. The location of the thin sections is given.

Thin section	Sampled interval	Analysed interval	Auppb	Pdppb	Ptppb	Ag	Al%	As	B	Ba	Be	Bi	Ca%	Cd	Ce	Co	Cr	Cu	Fe%	Ga	Ge	Hg	K%	La			
H0810-1	117,5-117,8	117,40-118,40	233	15	3	24,7	0,79	< 5	< 5	360	< 1	< 5	10,56	< 1	3	11	199	23401	1,25	< 5	< 2	1	0,58	6			
H0810-2	138,0-138,15	137,30-138,30	232	72	7	46,7	0,75	< 5	< 5	622	< 1	< 5	0,24	< 1	20	5	197	40117	0,84	< 5	< 2	2	0,54	13			
H0810-3A/B	138,15-138,23																										
H0810-6	135,8-136,0	135,70-136,48	40	6	4	8,8	0,45	< 5	< 5	53	< 1	< 5	15,75	< 1	8	11	105	7996	1,50	< 5	< 2	< 1	0,36	11			
H0810-9	136,24-136,36																										
H0810-10	136,36-136,48																										
H0811-11	139,2-139,5	139,10-140,20	112	8	6	36,9	0,69	< 5	< 5	1071	< 1	< 5	5,07	< 1	10	8	301	32330	1,02	< 5	< 2	5	0,64	8			
H0811-13	142,5-142,65	142,10-143,10	349	4	-2	11,1	0,43	< 5	< 5	369	< 1	< 5	7,80	< 1	13	10	204	16912	0,90	< 5	< 2	2	0,43	9			
H0811-14	143,5-143,75	143,10-143,78	656	28	-2	20,2	0,42	< 5	< 5	866	< 1	< 5	3,78	< 1	14	11	262	36025	1,19	< 5	< 2	1	0,43	9			
H0811-15	144,0-144,1	143,78-144,40	697	684	1692	16,7	0,70	< 5	< 5	1233	< 1	< 5	1,90	< 1	15	15	236	32493	1,31	< 5	< 2	3	0,67	10			
H0811-16	144,1-144,2																										
H0814-17A/B	320,45-320,7	320,20-321,00	483	1430	1560	4,9	1,44	< 5		3040	< 0,5	< 2	22,5	< 0,5		6	15	5960	0,76	< 10			0,61	20			
H0814-19	321,2-321,32	321,00-322,00	75	61	55	14,6	3,28	< 5		1230	< 0,5	< 2	17,35	< 0,5		8	28	6870	0,82	< 10			1,47	10			
H0821-20	127,4-127,6	127,00-127,80	1700	464	202	35,7	5,63	< 5		670	1,2	3	2,8	< 0,5		20	84	34100	1,66	10			2,55	10			
Thin section	Li	Mg%	Mn	Mo	Na%	Nb	Ni	P%	Pb	Rb	S%	Sb	Sc	Se	Sn	Sr	Ta	Te	Th	Ti	Tl	U	V	W	Y	Zn	Zr
H0810-1	7	2,54	5189	2	0,06	7	10	0,035	< 3	< 50	0,88	< 5	2	10	< 5	137	< 2	< 5	7	450	< 5	< 5	19	< 5	7	19	29
H0810-2	4	0,33	57	4	0,08	< 5	13	0,096	< 3	< 50	1,00	< 5	2	10	< 5	16	< 2	< 5	10	188	< 5	< 5	17	< 5	8	7	67
H0810-3A/B																											
H0810-6	5	6,26	11034	< 1	0,02	10	12	0,026	< 3	< 50	0,25	< 5	2	10	< 5	156	< 2	< 5	6	177	< 5	13	9	< 5	9	17	19
H0810-9																											
H0810-10																											
H0811-11	7	0,53	1667	26	0,10	< 5	16	0,073	< 3	< 50	0,86	< 5	2	10	< 5	63	< 2	< 5	11	340	< 5	10	11	< 5	5	9	45
H0811-13	5	0,53	2098	< 1	0,06	< 5	18	0,049	< 3	< 50	0,53	< 5	3	10	< 5	94	< 2	< 5	12	379	< 5	7	25	< 5	7	9	43
H0811-14	5	0,46	1045	2	0,11	< 5	23	0,059	< 3	< 50	0,98	< 5	2	10	< 5	51	< 2	< 5	8	364	< 5	8	19	< 5	5	10	34
H0811-15	8	0,65	531	6	0,13	< 5	32	0,081	< 3	< 50	0,91	< 5	3	16	< 5	32	< 2	< 5	10	540	< 5	9	28	< 5	8	12	66
H0811-16																											
H0814-17A/B	0,71	6160	2	0,68		7	0,012	4	0,27	< 5	2				437		< 20	500	< 10	10	17	< 10		5			
H0814-19	0,86	4480	8	1,56		10	0,026	6	0,26	< 5	3				275		< 20	800	< 10	20	27	< 10		8			
H0821-20	2,12	1410	3	2		22	0,049	2	0,79	< 5	7				57		< 20	1500	< 10	10	65	< 10		24			

Appendix 2: Chemical composition of minerals based on SEM analyses and normalised to 100 weight%. Stoichiometric values from <http://webmineral.com/chemical.shtml>.

Sperrylite PtAs₂				Isomertieite - Pd₁₁Sb₂As₂			
Sample	Pt %	Pd %	As %	Sample	Pd %	Sb %	As %
H0811-15	57.56		42.44	H0814-17B	73.98	16.34	9.69
	57.90		42.10		74.05	16.23	9.72
	57.48		42.52		75.01	14.15	10.84
	57.98		42.02	Average #3	75.93	14.36	9.72
	55.79		44.21	<i>Stoichiometric</i>	74.85	15.57	9.58
	56.78		43.22				
	55.46		44.54	Electrum - AuAg			
	57.86		42.14	Sample	Ag %	Au %	
	59.08		40.92	H0811-13	47.30	52.70	
	58.16		41.84		51.43	48.57	
	57.88		42.12		70.30	29.70	
	58.35		41.65		75.63	24.37	
	55.18		44.82	H0814-17A	68.42	31.58	
	56.21		43.79		75.65	24.35	
	56.42		43.58				
	57.82		42.18	Amalgam - AgAuHg			
	54.69		45.31	Sample	Ag %	Au %	Hg %
	50.98		49.02	H0814-17B	56.01	12.77	31.22
	58.81		41.19		57.36	11.16	31.47
	56.74		43.26		67.50		32.50
	59.39		40.61		66.35		33.65
	57.89		42.11		63.07		36.93
	56.94		43.06		64.48		35.52
	60.07		39.93		63.43		36.57
	58.43		41.57		63.41		36.59
	58.00		42.00		64.03		35.97
	55.18		44.82				
	58.67		41.33	Hessite Ag₂Te			
	59.05		40.95	Sample	Ag %	Te %	
	59.52		40.48	H0811-15	59.63	40.37	
	57.95		42.05		59.97	40.03	
	56.16		43.84	H0814-17A	57.28	42.72	
	58.00		42.00	<i>Stoichiometric</i>	62.84	37.16	
	55.07		44.93				
	57.40		42.60				
	59.95		40.05				
	55.61		44.39				
	53.36		46.64				
H0814-17A	55.48		44.52				
	53.37	4.05	42.58				
H0814-17B	60.26	3.12	36.62				
	60.70		39.30				
	62.28	2.04	35.68				
	62.62		37.38				
Average #44	57.47		42.33				
<i>Stoichiometric</i>	56.56		43.44				

Clausthalite - PbSe				Carrollite - Cu(Co,Ni) ₂ S ₄				
Sample	Ag %	Pb %	Se %	Sample	Cu %	Co %	Ni %	S %
H0814-17B		88.13	11.87	H0821-20	16.99	35.71	4.56	42.74
		89.93	10.07		18.75	35.12	4.06	42.07
	2.88	75.35	21.77		18.22	36.12	2.81	42.85
		78.59	21.41	Average #3	17.99	35.65	3.81	42.55
		78.11	21.89	<i>Stoichiometric</i>	<i>20.53</i>	<i>28.56</i>	<i>9.48</i>	<i>41.43</i>
		77.06	22.94					
		76.11	23.89	Cobaltite - CoAsS				
	3.04	74.53	22.42	Sample	Co %	As %	S %	
	4.25	73.24	22.51	H0811-15	36.20	35.56	28.24	
	3.09	71.71	25.20		34.77	38.38	26.85	
		72.32	27.68		34.56	36.61	28.83	
		77.32	22.68		32.79	39.66	27.55	
	4.09	69.77	26.14		33.93	39.28	26.79	
		77.09	22.91		33.26	39.07	27.67	
		76.65	23.35		34.33	39.51	26.16	
		79.24	20.76		34.62	39.21	26.17	
		79.44	20.56		32.08	38.91	29.01	
		78.15	21.85	Average #9	34.06	38.47	27.48	
	2.53	64.74	18.02	<i>Stoichiometric</i>	<i>35.52</i>	<i>45.16</i>	<i>19.33</i>	
	2.01	73.65	24.34					
	3.08	70.53	26.38					
	2.85	60.89	23.12					
	2.97	74.71	22.32					
	2.01	76.67	21.32					
	3.31	73.16	23.53					
	3.14	73.58	23.27					
	3.31	73.87	22.82					
Average #27	3.04	75.35	22.04					
<i>Stoichiometric</i>		<i>72.41</i>	<i>27.59</i>					
Bohdanowiczite								
Sample	Ag %	Bi %	Se %					
H0814-17B	15.86	50.84	33.30					
	24.12	42.71	33.17					
	24.92	39.05	36.03					
	25.35	41.71	32.94					
	23.80	42.10	34.11					
	20.67	44.73	34.59					
	20.06	42.59	37.35					
	20.16	44.66	35.18					
Average #8	21.87	43.55	34.58					
<i>Stoichiometric</i>	<i>22.72</i>	<i>44.02</i>	<i>33.26</i>					

Wittichenite - Cu ₃ BiS ₃								
Sample	Cu %	Bi %	S %		Sample	Cu %	Bi %	S %
H0811-16	38.87	38.93	22.20		H0814-17B	46.02	31.43	22.54
H0814-17A	52.84	24.05	23.10			45.32	32.60	22.08
	42.63	28.97	28.40			44.44	33.86	21.69
	50.04	27.89	22.07			44.53	33.53	21.94
	48.92	28.65	22.44			45.62	32.09	22.30
	45.08	31.92	23.00			42.90	35.12	21.97
	43.81	33.94	22.25			43.22	34.48	22.30
	46.82	32.08	21.09			41.94	34.36	23.70
	40.61	37.36	22.03			46.46	30.52	23.01
	42.08	35.31	22.60			42.44	35.40	22.16
	41.05	37.59	21.36			44.60	34.17	21.22
	46.63	30.20	23.17			41.89	36.59	21.52
	41.94	34.86	23.20			43.33	35.61	21.05
	42.29	35.06	22.65			44.90	32.41	22.69
	45.17	32.99	21.84			50.70	26.65	22.65
	50.61	27.48	21.91			48.81	28.20	22.99
	50.41	28.27	21.32			43.16	33.75	23.09
	41.70	38.39	19.91		H0821-20	41.80	36.02	22.18
	42.65	36.91	20.45			41.11	34.87	24.03
	42.71	35.67	21.61		Average #66	43.95	33.37	22.67
	42.94	34.59	22.47		<i>Stoichiometric</i>	38.45	42.25	19.40
	42.34	35.63	22.03					
	42.67	34.97	22.36					
	48.57	29.20	22.23					
	41.76	35.63	22.62					
	39.39	36.93	23.67					
	46.21	32.12	21.67					
	41.46	35.98	22.56					
	39.39	37.84	22.77					
	38.66	36.83	24.51					
	41.19	36.51	22.30					
	37.68	38.17	24.15					
	42.14	33.97	23.89					
	39.87	34.80	25.33					
	46.22	30.56	23.22					
	42.10	36.10	21.80					
	48.05	27.58	24.36					
	39.71	36.94	23.35					
	44.57	32.79	22.65					
	39.99	37.59	22.42					
	43.15	35.44	21.41					
	46.79	28.78	24.43					
	43.40	33.89	22.71					
	42.48	36.76	20.75					
	48.99	24.75	26.26					
	47,30	28,62	24,08					
	43,81	31,57	24,63					



Norges geologiske undersøkelse
Postboks 6315, Sluppen
7491 Trondheim, Norge

Besøksadresse
Leiv Eirikssons vei 39, 7040 Trondheim

Telefon 73 90 40 00
Telefax 73 92 16 20
E-post ngu@ngu.no
Nettside www.ngu.no

*Geological Survey of Norway
PO Box 6315, Sluppen
7491 Trondheim, Norway*

*Visitor address
Leiv Eirikssons vei 39, 7040 Trondheim*

*Tel (+ 47) 73 90 40 00
Fax (+ 47) 73 92 16 20
E-mail ngu@ngu.no
Web www.ngu.no/en-gb/*